Strip hit resolution of CMS Tracker analysis

Thesis · June 2017

DOI: 10.13140/RG.2.2.11136.84480

1 author:

Mohamed Elashri
University of Cincinnati
4 PUBLICATIONS **0** CITATIONS

SEE PROFILE

Bachelor Thesis
High Energy Physics
June 2017

Strip Resolution of CMS Tracker Study

Mohamed Elashri

Dept. Physics of Earth & Universe
University of Science and Technology
Giza, Egypt

This thesis is submitted to the Department of Physics of Earth & Universe at University of Science and technology- Zewail City in partial fulfillment of the requirements for the degree of Bachelor of Science in High Energy Physics.

Contact Information:
Author:
Mohamed Elashri
E-mail:
s-mohamed.elashri@zewailcity.edu.eg

University advisor:
Prof. Ahmed Abdelaim
Prof. Amr Mohamed
Dept. Physics of Earth & Universe

Dept. Physics of Earth & Universe
University of Science and Technology- Zewail City
Giza, Egypt

Internet : www.zewailcity.edu.eg
Phone : +02 385 40 400

Acknowledgments

I would like to extend my gratitude first and foremost to my first thesis advisor Dr.Ahmed Abdelalim for mentoring me over the course of my undergraduate study and my graduation project period. He has helped me through extremely difficult times over the course of the analysis and the writing of the thesis and for that I sincerely thank him for his confidence in me.

I would like also extend my gratitude to my second thesis advisor Dr.Amr Mohamed for all support he gives me during the period of study and his helpful opinions about the subject.

I would additionally like to thank Dr. Nicola De Filippis (University Of Bari , Italy) for useful discussion about CMS Tracker and his great inspiration of the Tracker Study.

I would also like to extend my appreciation to Ms.Nada Khaled as she held the task of reviewing the thesis and check if the thesis language is obvious enough.

Finally I would like to extend my deepest gratitude to my parents as without whose love, support and understanding I could never have completed this degree.

Abstract

The CMS silicon tracker consists of two tracking devices utilizing semiconductor technology: the inner pixel and the outer strip detectors. They operate in a high-occupancy and high-radiation environment presented by particle collisions in the LHC. The tracker detectors occupy the region around the center of CMS, where the LHC beams collide, between 4 cm and 110 cm in radius and up to 280 cm along the beam axis. The pixel detector consists of 66 million pixels, covering about 1 m^2 total area. It is surrounded by the strip tracker with 10 million read-out channels covering about 200 m^2 total area. In this study, details are given about the performance of the strip tracker at high occupancy with respect to local observables such as signal to noise ratio and hit reconstruction efficiency. Studies of strip hit resolution that affects the quality of track reconstruction.

Keywords: CMS, Large Hadron collider, Detector, Strip Tracker.

Contents

List of Figures

List of Tables

Chapter 1

Large Hadron Collider

1.1 Introduction

The Large Hadron Collider (LHC) is the world's biggest and powerful particle accelerator that ever built. it is a circular hadron-hadron collider operated at CERN,[1] between the Jura mountain range in France and Lake Geneva in Switzerland. The accelerator have a circumference of 26.7 kilometres and located in the underground tunnel that is buried 170 m underground which was originally constructed to host the Large Electron Positron (LEP) Collider [2] which was operating in the period from 1989 to 2000. A diagram of the LHC is shown in Figure 1.1 . The main part of the LHC program is to operate as a proton-proton *(pp)* collider , while part of the machine schedule is to deliver heavy-ion collisions. The LHC collides protons at four locations along the ring of the machine, corresponding to the location of the four LHC experiments: ATLAS [3], CMS [4] Alice [5], and LHCb [6]. In chapter 2 we are going to discuss the CMS experiment in more details.
Inside LHC the proton beams travels in opposite directions in separate beam pipes. They are guided inside the beam with a strong magnetic field created by super conducting magnets. Protons used in the collisions are obtained from hydrogen gas atoms. This protons begin the chain process in a linear accelerator called lineac2 which is the starting point for the protons used in experiments at LHC , lineac2 replaced lineac1 in 1978, it accelerates the protons to 50 MeV .Then the protons are injected in to the PS Booster which is four superimposed synchrotron rings that receive beams of protons from the Linac 2 and accelerate them to 1.4 GeV, after this stage protons are send to Proton Synchrotron where they are accelerated to 25 Gev. Then they are sent to Super Proton Synchrotron (SPS) where they are accelerated to about 450 Gev. Finally they are injected into LHC where they are accelerated to their final energy, after that collisions occurs which can take many hours at a time. This accelerating scheme results in circulating the ring in bunches by the proton beam, under normal working conditions, each proton beam has 2808 bunches, with each bunch containing about 10^{11} protons [8]. They are few centimeters long and 16 μM wide whey the collide. As a consequence each bunch crossing produce produce many *pp* interactions. Final stage is designed to accelerate particles to center-of-mass energies of 14 TeV (7 TeV per beam). Currently it works only at the center of mass energy of 13 TeV.

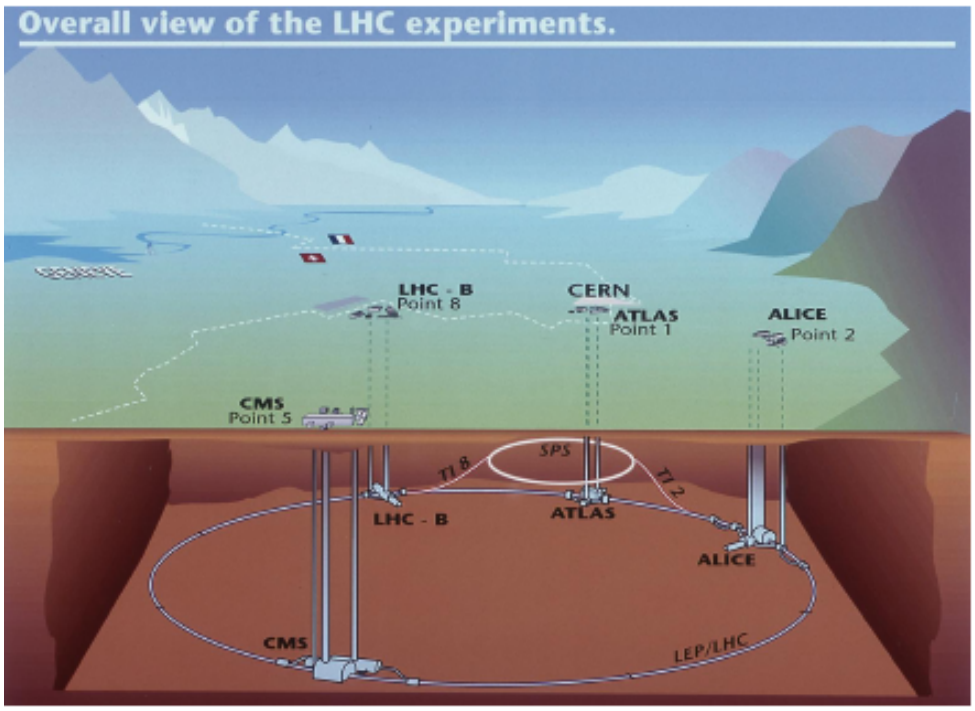

Figure 1.1: Diagram of the locations of the LHC's four main experiments (ALICE, ATLAS, CMS and LHCb):

The Large Hadron Collider (LHC) is designed to study the *pp* collisions at a center of mass energy 14 TeV with a luminosity up to $10^{34} cm^{-2} s^{-1}$. However heavy ion collisions (lead-lead for example) are also studied at the LHC. The main features of the accelerator are summarized in the Table 1.1
LHC project has its computing model which has the aim of constructing and maintaining a distributed data storage. This is open for all the LHC community that uses a large amount of data produced by the LHC Experiments. This is called LHC Computing Grid based on Grid technologies [11]. But this presents many challenges , one is related to the storage as LHC produces roughly about 15 Peta Byte (PB) of raw data every year which arise a real problem of how to deal with it. Another challenge is the fact that there are huge number of people working in the LHC community spread all over the world want to access these data t simultaneously. In LHC Grid these is hierarchy based on sites called Tiers. Primary backup of data is recorded at CERN which is the unique Tier0 center. After initial processing, these data are distributed to a series of Tier1 centers (13 center worldwide). Each Tier1 center defines a cloud which makes data available to the Tier2 centers within their clouds.

Parameter	Value
Circumference (km)	26.7
Beam Energy (TeV)	7
Number of magnet dipoles	1232
Magnet Temperature (Kelvin)	1.96
Maximal number of bunches	2,808
Protons per bunch	$1.05 * 10^{11}$
Bunch length |cm|	7.5
Bunch spacing (ns)	25
Maximum Luminosity $10^{34} cm^{-2} s^{-1}$	10^{34}

Table 1.1: : The Large Hadron Collider (LHC) designed parameters for nominal operation [10]

A detailed overview of the LHC (from which much of the material in the following sections is obtained) may be found in [9]

1.2 layout

The LHC is divided into 8 octant separated by 8 insertion points which occupied with 8 experiments. For the aim of colliding particles with the same charge, the two hadron beams are kept separate, in most parts of the LHC. The clockwise and counter-clockwise rotating beams, refereed to Beam 1 (B1) and Beam 2 (B2) are only brought together in the four interaction points shown in Fig 1.1.

1.3 Magnets

The LHC , The magnetic field is used for bending and focusing the particle on their circular trajectory. Charged particle momentum p describe circle with radius R inside a homogeneous magnetic field B can be related according to the following relation:

$$p_{max} = q \cdot RB_{max} \tag{1.1}$$

where q is the particle's charge. And the quantity $RB = \frac{p}{q}$ is called magnetic rigidity, which is used to normalise the equation to make them momentum independent. In LHC, the magnetic bending radius is $R \approx 2804m$. The magnetic field needed for the high required beam momentum is high. For fulfilling 7 TeV momentum beam, a magnetic field of at least 8.33 T is required. This relativity high magnetic field can be only obtained using superconducting magnets. The magnetic field of the superconducting magnets is defined by the current distribution around the bores. It can be obtained from the relation:

$$B(r,\Phi) = -\frac{\mu_0 I_0}{2a}\left(\frac{r}{a}\right)^{n-1} \cdot [sin(n\Phi), cos(n\Phi)] \tag{1.2}$$

where r is the distance to the magnetic centre, Φ is the angle with the horizontal plane and n is the multipole order.In LHC, the requirement of the minimising the occupied space inside the tunnel and costs reduction imposed a constrains on the design of magnets. In Fig 1.2 a two chosen designs in the LHC are shown. The superconducting magnetic field distribution is primarily determined by the position, shape of the the fields inside the coils.
The LHC superconducting magnets are kept in a liquid helium bath to keep them at the required low temperature to sustain the superconductivity property. Liquid nitrogen and a vacuum tank are used to isolate the Liquid helium, and they are kept in steel tubes for protection purpose.

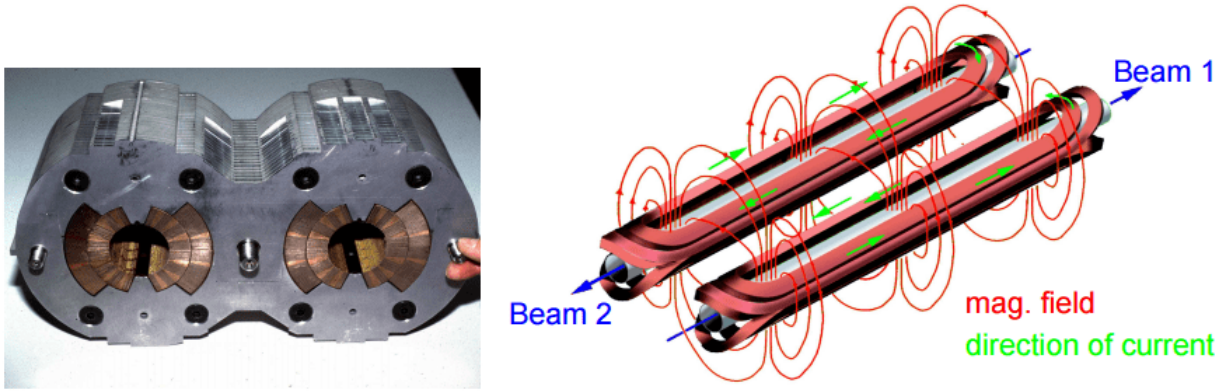

(a) dipole cross section (b) dipole coil geometry

Figure 1.2: LHC main dipoles [27].

1.4 Luminosity

In High energy physics Experiments, the Luminosity is a measure of interactions per unit time per unit area. It gives the amount of data that produced during the collisions in the accelerator. And for a physics analysis requirement, a precise measurement of the integrated luminosity is required to convert observed number of events into cross-section which relates to probability of occurrence. However instantaneous luminosity can be used instead of the integrated luminosity. For a given process with cross section σ which producing number of events N, the instantaneous luminosity is defined to be

$$N = \sigma \mathcal{L} \tag{1.3}$$

The cross section (σ) of a physical process can be linked to the event rate through relation dN/dt via Luminosity $\mathcal{L}$ as [12]:

$$\frac{\mathrm{d}N}{\mathrm{d}t} = \mathcal{L} \times \sigma \tag{1.4}$$

where σ depends on the center of mass ($\sqrt{s}$) , and the instantaneous luminosity at the LHC is given by

$$\mathcal{L} = \frac{N_b^2 n_b \mathcal{F}_{rev} \gamma_r}{4\pi\epsilon_n \beta*} F \tag{1.5}$$

where N_b is the number of protons per bunch ($\sim 10^{11}$) , n_b is the number of bunches in each beam ($\sim 10^3$) , $\mathcal{F}_{rev}$ is the number of times per second that the beam travels around the ring (1 kHz), γ_r is the relativistic gamma factor ($\sim$ 7000), ϵ_n is the normalized transverse emittance ($\sim 4\mu m$), $\beta*$ is the beta function at the interaction point, F is the geometric Luminosity reduction factor which is due to the crossing angle. This factor can be calculated by

$$F = (1 + (\frac{\theta_c \sigma_z}{2\sigma*})) \tag{1.6}$$

where θ_c is the full crossing angle at interaction point, σ_z is the root-mean-square of the bunch length, and $\sigma*$ is the transverse root mean square of the beam size at the interaction point. Equations 1.2 and 1.3 requires $\sigma_z \ll \beta$. Then the integrated luminosity can be obtained from instantaneous luminosity, as the integrated luminosity is defined as the time integral of instantaneous luminosity

$$L = \int \mathcal{L} dt \tag{1.7}$$

From equations above it can be deduced that in order to achieve the high design luminosity of $\mathcal{L} = 10^{34} cm^{-2} s^{-1}$, high beam intensities have to be obtained. These intensities can not be achieved with anti-protons. To allow proton-proton collisions, two magnetic dipoles fields separated from each other are user to steer the particles through LHC machine. The beams are separated then in individual beam pipes and brought together at the interaction points. This dipoles and strong magnets installed at each interaction points brings highly focused beams to collision.
Instantaneous luminosity decays over the course of the LHC machine run. This is due to the beam losses. There are many reasons for this losses, it could arises from collisions itself, interaction with rest gas in the beam pipe and intrabeam scattering. the decay is exponential in order so the integrated luminosity can be calculated from the instantaneous luminosity taking into account the losses by the relation

$$L = \mathcal{L}_0 \tau (1 - e^{\frac{T_{run}}{\tau}}) \tag{1.8}$$

where $\mathcal{L}_0$ is the initial instantaneous luminosity , T_{run} is the integrated run time and τ is the luminosity lifetime. The integrated luminosity optimized taking into account the degradation of the initial instantaneous luminosity and the LHC refill time.

1.5 Large Hadron Collider Main Experiments

1.5.1 Compact Muon Solenoid

The Compact Muon Solenoid (CMS) experiment is a general purpose particle physics experiment in LHC. The CMS detector designed to allow for all reconstruction of all types of (detectable) particles produced in the hadron-hadron collisions in LHC. This open possibility to perform wide range of measurements, from the Standard model precision measurements to search for new physics. The idea behind the CMS detector is the configuration of the magnetic field needed to bend the trajectory of the charged particles produced in the collision, especially muons, allowing for the accurate measurement of their momentum. The detector all components are compact enough to be located inside of the superconducting solenoid. Figure (1.3) shows an illustration of the CMS detector and its subsystems. Chapter 2 is devoted to the a more detailed discussion on CMS Experiment.

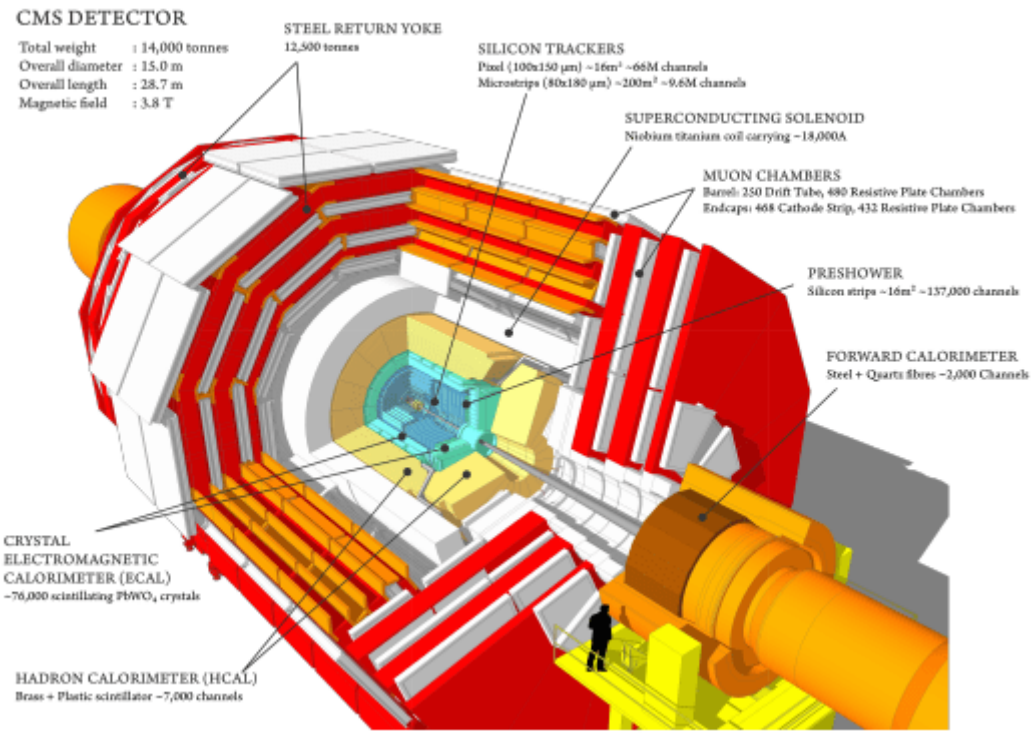

Figure 1.3: Graphic representation of the CMS detector and its subsystems.

1.5.2 Large Hadron Collider Beauty

The Large Hadron Collider Beauty (LHCb) primary aim is to investigate the decay of **B**-particles (particles contains b quarks) and to give the insight about the matter-antimatter asymmetries phenomenon. The LHCb detector, Fig(1.4) is a forward spectrometer designed to take advantages of the characteristic $b\bar{b}$ pair angular distribution. The detector length is about 20 m and the total dimensions are about $6 \times 5 \times 20\, m^3$. The detector covers the range from 15 mrad to 300 mrad in the bending and from 15 mrad to 250 mrad in the non bending plane. The spectrometer magnet provides an integrated field of about 4Tm deflecting charged particles in the horizontal plane. The magnet influences the proton beams and three dipole magnets are dedicated to compensate the effect and stabilise the beams.

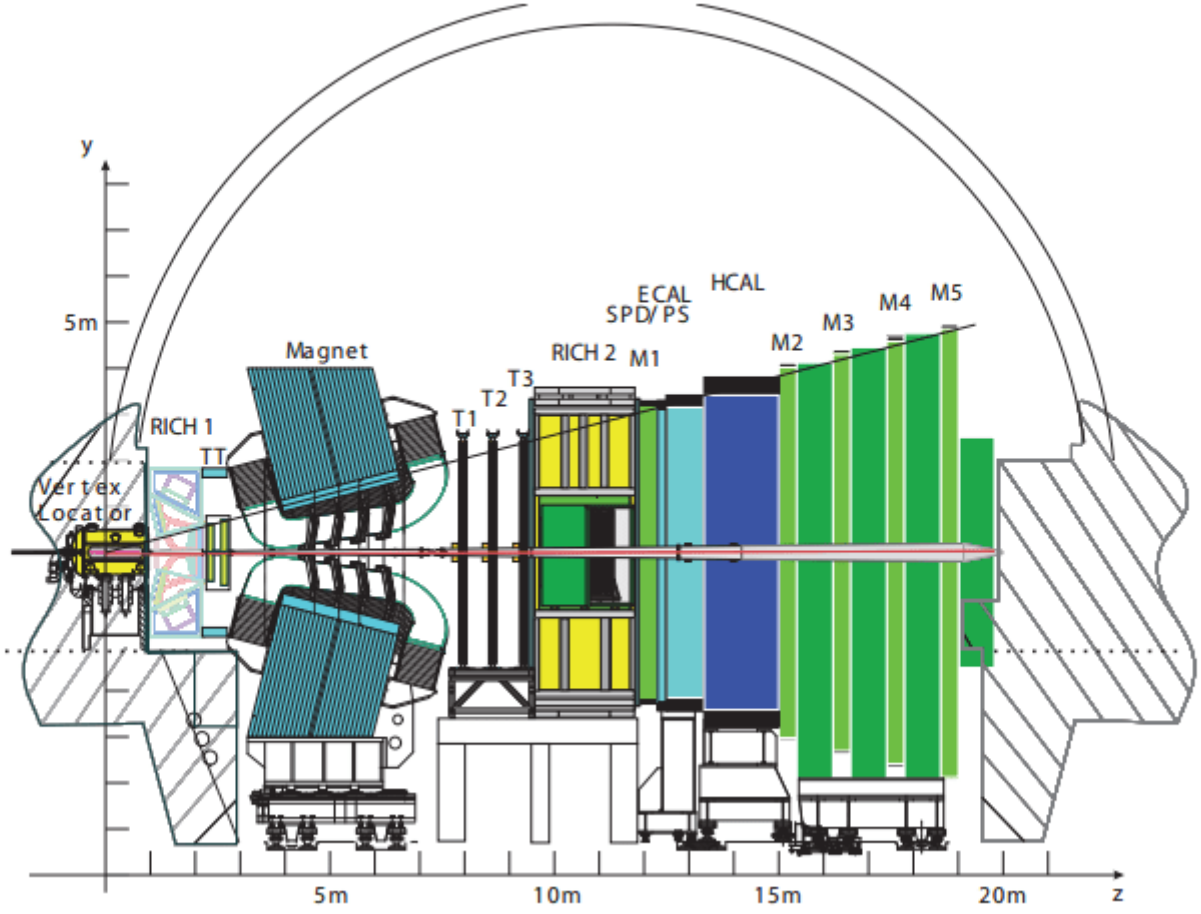

Figure 1.4: The LHCb detector: side view.

1.5.3 A Large Ion Collider Experiment

A Large Ion Collider Experiment (ALICE) is an experiment at the LHC dedicated to heavy-ion physics, residing in the experimental cavern of the previous L3 experiment. It is aiming at re-creating the conditions of the early universe before the on-set of confinement and to study the properties of the QGP. Most of its sub-detectors are confined inside the L3-magnet. With a magnetic field strength up to about 0.5 Tesla, it is the largest conventional magnet of its size. The magnetic field is parallel to the z-axis. Figure 1.5 shows cut-through view of the ALICE detector.

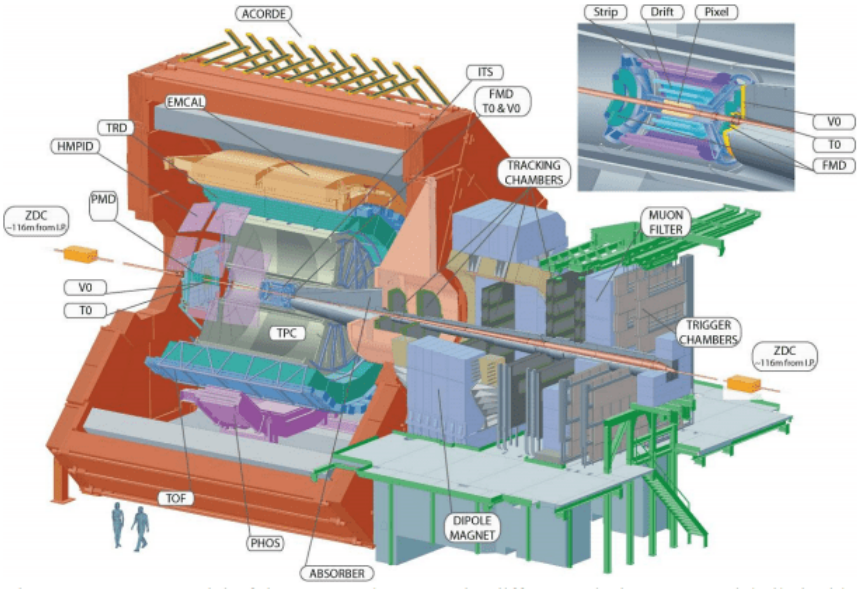

Figure 1.5: Schematic view of ALICE detector.

1.5.4 A Toroidal LHC ApparatuS

Chapter 2

Compact Muon Solenoid

2.1 Introduction

In this chapter the different components of the Compact Muon Solenoid (CMS) experiment and detector will be described. The Compact muon solenoid [13], (Fig 2.1) is designed as a general purpose detector aimed to achieve the physics goals of LHC. Main feature of CMS is a superconductor that provides a magnetic field of 3.8 T over a magnetic length of 12.5 and a free-bore radius of 3.15. CMS is 28.7 m and weights about 14000 tonnes.The detector is designed to allow for the reconstruction of different types of detectable particles produced in Hadron-Hadron collisions delivered by LHC, opening the possibility of performing wide range of physics measurements and discoveries. This means that it can used for precision tests of the Standard Model (SM) and to search for new physics[14]. The main idea driving the design of the detector is the conguration of the magnetic field needed to bend the trajectory of charged particles that produced in LHC collisions , especially muons , This allow for accurate measurement of their momentum. There are several detector requirements for CMS to meet these goals[14]:

- Good muon identication and momentum resolution over a wide range of momenta, good dimuon mass resolution ($\approx 1\%$ at 100 Gev) and the ability to unambiguously determine the charge of muons with p < 1 TeV
- Good charged particle momentum resolution and reconstruction efciency in the inner tracker. Efcient triggering and ofine identication of τ leptons and b-jets, requiring pixel detectors close to the interaction region
- Good electromagnetic energy resolution, good diphoton and dielecron mass resolution ($\approx 1\%$ at 100 Gev), wide geometric coverage, π^0 rejection, and efcient photon and lepton isolation at high luminosities
- Good missing-transverse-energy and dijet-mass resolution, requiring hadron calorimeters with hermetic geometric coverage and ne lateral segmentation

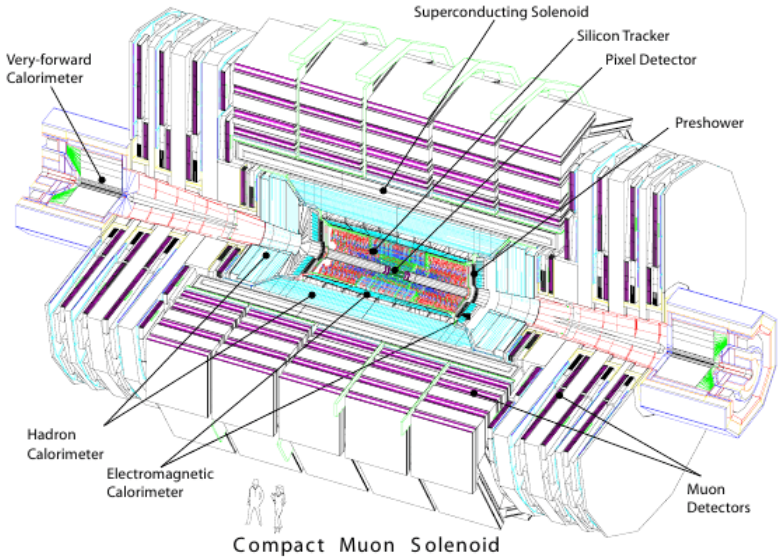

Figure 2.1: Perspective view of the CMS detector[15].

- Fast online event selection processes (triggers) to reduce the rate from 10^9 inelastic collision events per second to $\lesssim$ 1000 events per second for storage and subsequent analysis
- Infrastructure for the alignment and calibration of the detector

The design of CMS, shown in Fig. 2.1 and detailed in the following sections, meets these requirements. Each detector subsystem is integral to the performance of CMS as a whole and is specialized to a particular class of particles , as seen in Fig 2.2,the silicon tracker is designed to allow a good identification of charged particles tracks , the electromagnetic calorimeter was designed to measure electromagnetic showers with a good energy resolution to allow good di-photon and di-electron mass resolutions, the hadron calorimeter measures the energy of charged and neutral hadrons, and the muon detectors identify and measure the momentum of muons. The large bending power (11.4 T m) of the superconducting magnet permits a precise measurement of the momentum of high-energy charged particles in silicon tracker. The return eld is large enough to saturate 1.5 m of iron, allowing four muon stations to be integrated and the bore of the magnet coil is large enough to accommodate the inner tracker and the calorimetry inside, thereby reducing the amount of material in front of the calorimeters[14].

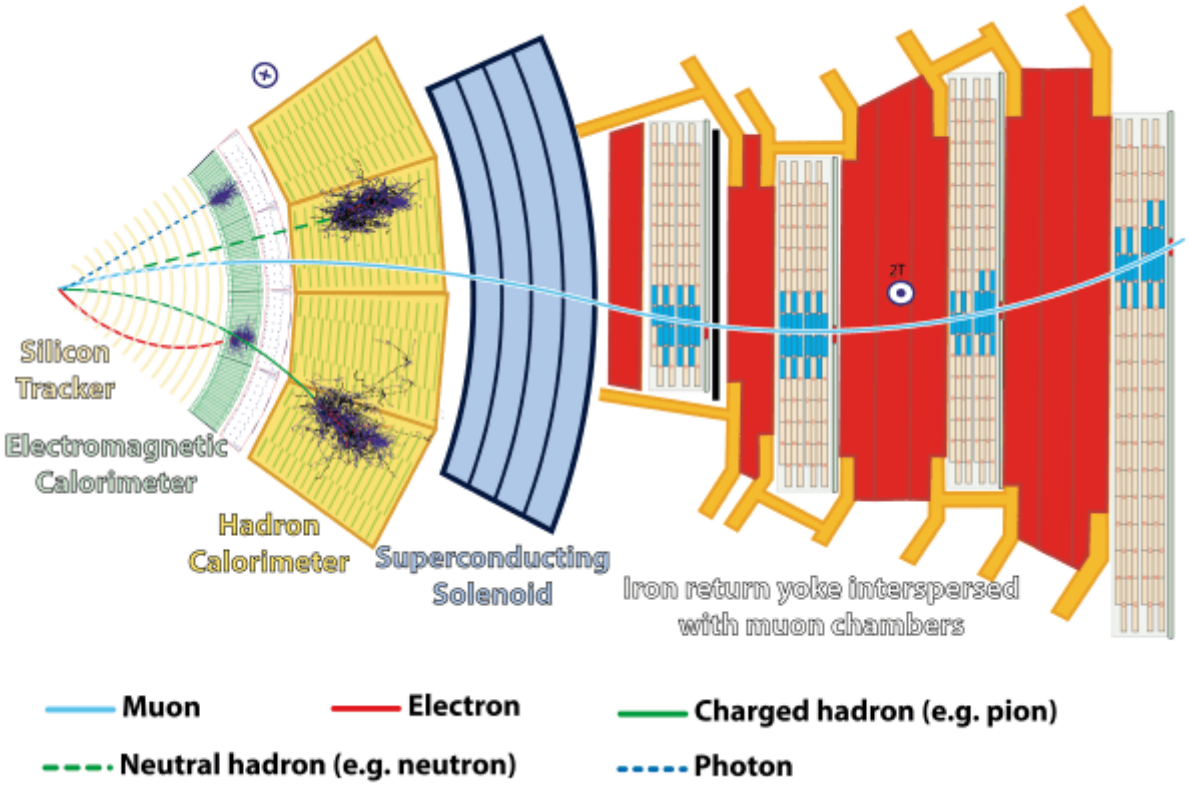

Figure 2.2: A slice of the CMS detector[15].

2.2 Coordinate System

For to construction and measurements of an event , it is useful to define a coordinate system which origin is the collision point. This is done in CMS with the following convention using Cartesian coordinate system [16]:

- the x-axis points toward the LHC ring center,
- the y-axis points upward, toward the surface,
- the z-axis coincides with the CMS cylinder axis.

Using the cylindrical symmetry of CMS allows to introduce pseudo-angular reference coordinate system given by parameters (r,ϕ,η), where r is the radial distance from beam axis, ϕ is azimuthal angle measured with respect to the x-axis in the x-y plane and η represents the angular distribution in the apparatus and also know as the pseudo-rapidity to rapidity (ξ) , which is defined as follows:

$$\eta = -\ln \tan \frac{\theta}{2} \tag{2.1}$$

where θ is the polar angle with respect to z-axis.There is advantage for using the pseudo-rapidity instead of the polar angle is that over an equal distance in η the particle flux is approximately constant and $\triangle\eta$ between any two vectors is Lorentz invariant. Pseudo-rapidity for high energy particles can be approximated to

$$\xi = \frac{1}{2} \ln \frac{E + P_z}{E - P_z} \tag{2.2}$$

where E is the outgoing particles energy , P_z is the momentum of the projected particle along beam z-axis. And due to Lorentz invariance property , rapidity is the variable of interest at hadron colliders.The transverse momentum P_T relative to beam direction is computed from the x- and y- components, while transversed energy E_T is computed as

$$E_T = E \sin \theta \tag{2.3}$$

2.3 Superconducting magnet

The CMS detector has a powerful superconducting solenoid (3.8 T), because of the high energy of colliding beams it also produces particles with high energies. And for the measurement of momentum and tracks of these particles, a strong magnetic field if required. The task of the CMS magnet is to bend the charged particles. The higher of the momentum of the particle is , the less it bends under the influence of magnetic field. Thus the measurements of the momentum can be obtained from the curvature of the particle trajectory. And the direction of bending gives the information about the charge of the particle. The CMS magnet Fig 2.3 has a solenoid structure with a 10000 ton return yoke. The magnet is cooled to $\approx$ 4.86 Kelvin to maintain superconductivity. It has a length of 12 m and it occupies the region 2.9 < r < 3.8 and $\left|\eta\right| < 1.5$. The magnetic field lines are closed by an external 21 m long iron yoke, that has a diameter of 14 m. In the return yoke a 1.8 T magnetic field is present, pointing at the opposite direction with respect to the internal field.

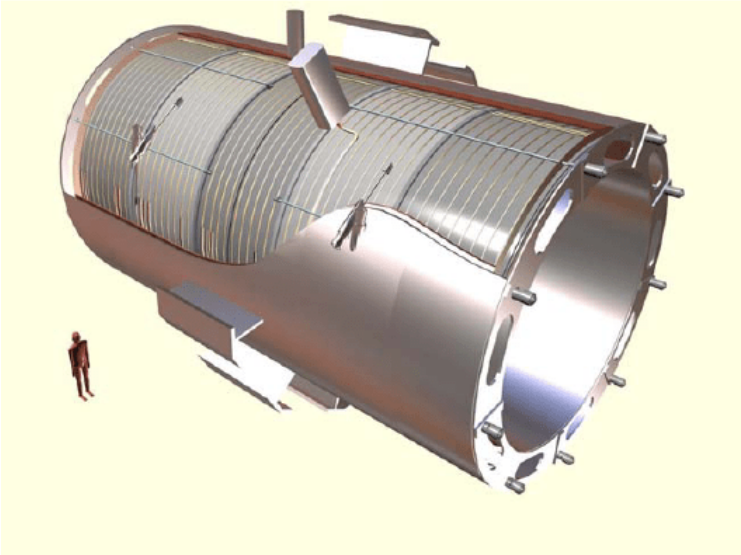

Figure 2.3: General artistic view of the 5 modules composing the cold mass inside the cryostat , with details of the supporting system[16].

The CMS magnet achieves the magnetic field of 3.8 T at a full current of 20,000 Amperes, and the energy stored in the magnet is 2.6 GJ. The flux is returned via iron yoke, which is a 5 barrel wheels 3 endcap disk on each side. The tracking of muons can be controlled through the magnetic field of the returned yoke, which is 1-2 T. And due to the possibility of magnetic superconductivity loss due to quenching , all the energy stored is dumbed to to resistors within a time of 200 sec. The CMS magnet system includes a vacuum pumping, cryogenic system,control system and a power supply.

2.4 Silicon Pixel Detector

The pixel detector is the most inner part of the CMS tracker. It covers range -2.5 $< |\eta| <$ 2.5.The pixel detector compused of the barrel part (BPIX) and the forward endcap discs (FPIX) , Fig 2.4. BPIX has a 53 cm length (in z-direction). It it a three concentric cylindric layers with radii 4.4, 7.3 and 10. 2 cm. The BPIX consists of 48 milion pixels in total. Each with a size of $100 \times 150\ \mu m^2$. This results in a pixel position of 15-20 μm^2 [18]. The FPIX discs has a radius from 6 cm to 15 cm, and placed on each side of BPIX at z ± 34.5 cm and z ± 46.5. The FPIX has a 18 million pixels of the same size as for the BPIX. The BPIX and FPIX are aligned in such manner that every particle crossing the tracker, will cross three different pixel layers for a wide η range. The CMS Pixel tracker wil be discussed in more detail in the next chapter.

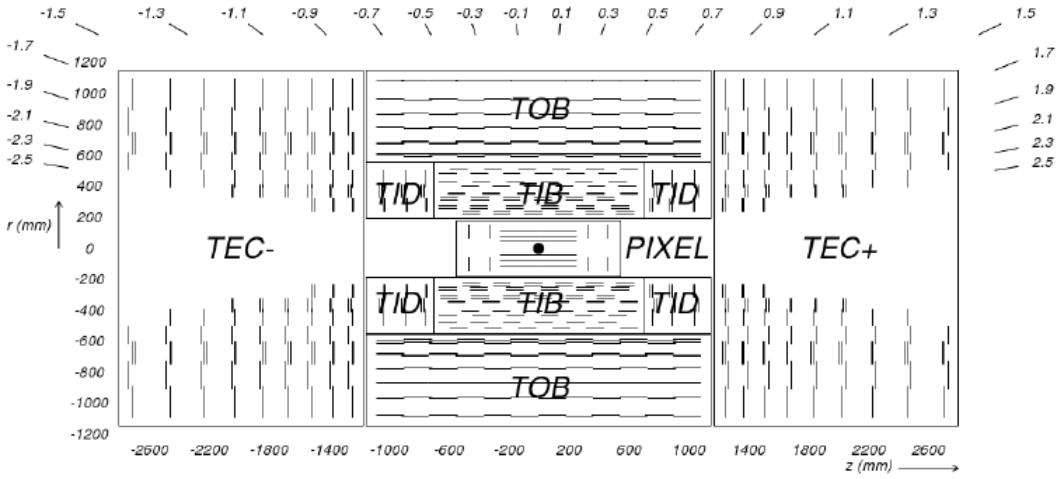

Figure 2.4: View of the CMS tracker in r z plane. It shows the pixel and the strip detectors. [17]

2.5 Silicon Microstrip Tracker

The strip tracker occupies 20 cm < r < 116, (see Fig 2.4). It contains from several parts , Tracker Outer Barrel (TOB) , Tracker Inner Barrel (TIB) , Tracker Inner Disc (TID) and Tracker EndCaps (TEC+ and TEC-, where the sign corresponds to the sign of the z-coordinate of the detector position). The TIB and TID has a radius extended to 55 cm.The TIB is consists of 4 layers and the TID consists of 4 discs on each side of TIB. The silicon strips in TIB and TID are of 320 μm thick. The TOB part is surrounding the TIB and the TID, and the TOB has a radius of 116 cm. The TOB consists of 4 layers each of 500 μm thick micro-strip sensors. The TOB with TID and TIB extnds in -116 cm < $|z|$ < 118 cm[20]. The TEC+ and the TEC- discs covers 124 cm <$|z|$ < 282 cm and 22.5 cm < r < 113.5 cm, and each TEC is a 9 discs with up to 7 rings of silicon micro-strip sensors for each. More discussion about silicon microstrip tracker in chapter 3.

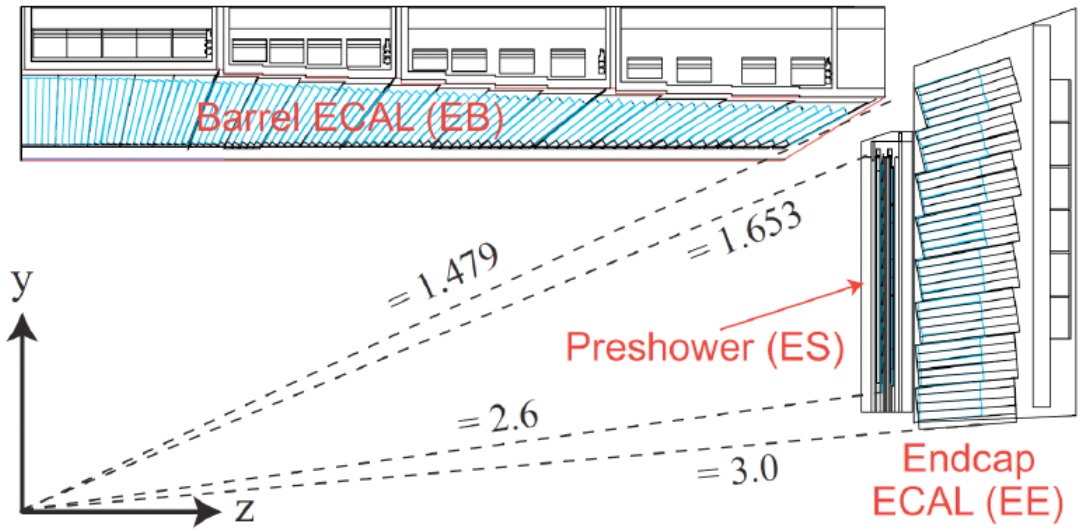

Figure 2.5: View of one quarter of the CMS ECAL. [19]

2.6 Electromagnetic Calorimeter

The main purpose of the Electromagnetic Calorimeter (ECAL) is to identify electrons and photons and to precisely measure their energies. Fig 2.6 shows the design of the ECAL. The CMS ECAL is hermetic homogeneous calorimeter with cylindrical geometry, composed of many scintillating crystals of lead tungstate ($PbWO_4$) with a truncated pyramidal shape. And it consists of two parts , The ECAL barrel (EB) , which contains about 61200 crystals , and two endcaps (EE) , which contains 7324 crystals each one. The $PbWO_4$ crystals were chosen as scintillators because of their short radiation lengths (X_0 = 0.89 cm) and Molie‘re radii (R_M= 2.2 cm).The scintillators are relatively fast, with 80% of the light being emitted within 25 ns.And radiation hard up to 10 Mrad.

The ECAL barrel (EB) is a 36 supermodules of half barrel length and this corresponds to a total coverage of $|\eta| < 1.479$, at a distance to the vertex of r = 129 cm.Each one of this supermodules consists of 4 modules. Each crystal is 230 mm long which translates to 25.8 radiation lengths.

The ECAL End-Caps (EE) has a coverage of $1.479 < |\eta| < 3.0$ and sitting at$|z|$= 314 cm. Each endcap consists of two semicircular aluminium halves which called *Dees*. The crystals in endcaps have a length of 22 cm , frontal area equals $28.6 \times 28.6\ mm^2$ and rear surface of $30 \times 30 mm^2$. The crystals in endcaps are arranged according to $\eta - \phi$ symmetry.The energy resolution of a homogeneous calorimeter can be expressed by the sum in quadrature of three terms, as shown in the following formula

$$\left(\frac{\sigma_E}{E}\right)^2 = \left(\frac{S}{\sqrt{E}}\right)^2 + \left(\frac{b}{E}\right)^2 + c^2 \tag{2.4}$$

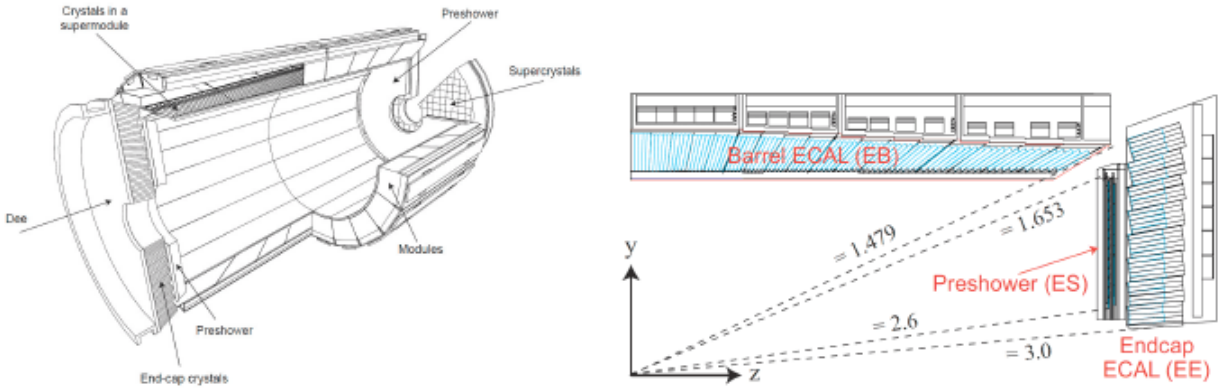

(a) r–z view of an ECAL sector. (b) ECAL three-dimensional view.

Figure 2.6: Schematic representation of the CMS electromagnetic calorimeter. [20]

where S term is the stochastic term dominates at low energies, and it includes the statistical uctuations contribution in the number of generated and collected photoelectrons. This term takes into account the crystal light emission, the light collection eciency and the photodetector quantum eciency (the ratio between the number of collected photoelectrons and the number of photons incident on the photodetector). And the b term is the noise term includes the contributions of pile-up events and electronic noise, both due to the photodetector and preamplier. These contributions depend on η and the **LHC** operational luminosity. The constant term c dominates at high energies , it takes into account many contributions. They are the nonuniformity of the longitudinal light collection, the intercalibration errors and the leakage of energy from the rear side of the crystal. Accroding to this fr EB resolution for electron was measured to be[20]:

$$\left(\frac{\sigma_E}{E}\right)^2 = \left(\frac{2.8\%\ GeV^{1/2}}{\sqrt{E}}\right)^2 + \left(\frac{12\%\ GeV}{E}\right)^2 + (0.3\%)^2 \tag{2.5}$$

where E is the energy measured in GeV.

2.7 Hadron Calorimeter

The CMS Hadron Calorimeter (HCAL), Fig 2.7 is used together with ECAL to make a complete a calorimetric system for the jet energy and direction measurement. It can measure energy imbalance in the transverse plane E_T^{miss}, which is a typical signature of non interacting particles such as neutrinos.The HCAL is covering the region $|\eta| < 5$ as shown in fig 2.7, it is divided into four subdetectors : HB (*Barrel Hadronic Calorimeter*) , located in the barrel region inside the solenoid with $|\eta| < 1.4$; HE (*Endcap Hadronic Calorimeter*) , placed in the endcaps region inside the magnet covering region $1.3 < |\eta| < 3$ and overlaps partially with HB coverage; HF (*Forward Hadronic Calorimeter*) consists of quartz bers sandwiched between iron absorbers, formed by two units placed in the region $3 < |\eta| < 5$ which is outside the magnetic coil/ This quartz fibers emits cherenkov light with the passage of the charged particlesand this light is detected by the radiation photomultipliers. The last part is the HO (*Outer Hadronic Calorimeter*), placed along the inner wall of magnetic field return yoke, which is just outside the magnet[20].

The HB calorimeter is segmented into 72×32 towers in $\phi \times \eta$ corresponding to size of $\triangle\Phi \times \triangle\eta = 0.087 \times 0.087$. Each tower consists of 155 mm thick brass plates interleaved with scintillator plates of a 3.7 mm thickness, except the first plate which is of thickness 9 mm.

The HO calorimeter consists of the aforementioned scintillators placed between magnet coil and muon system. They follow the geometry of the barrel muon detector, They are grouped in 60 degree sectors in ϕ and five rings in η. And the central ring have a 2 scintillator layers covering iron absorber sides, while the others are only one layer of scintillator.

The HE calorimeter covers the region $1.479 < |\eta| < 3$ as mentioned before . It is segmented into 13 towers in η and 72 in ϕ.. The layered construction of the HE is similar to that of the HB using 79 mm thick brass absorbers followed by plastic scintillators. The resolution of the HE towers is ($\triangle\eta, \triangle\phi$ = (0.087,0.087) for $|\eta| < 1.6$ and ($\triangle\eta, \triangle\phi$ = (0.17,0.17) for $|\eta| > 1.6$.

The HF calorimeter is a forward calorimeter detector located at a distance of 11.2 m from nominal interaction point outside the solenoid,and almost hermetic with very high missing transverse energy absorption. It consists of material of two units, the steel absorber and embedded radiation hard quartz fibers. It is segmented into 13 towers in η with a size of $\triangle\eta = 0.175$ except for lowest η tower where size is 0.1. And in Φ the towers have a size of 10° with the exception of the highest η tower that has double size[16].

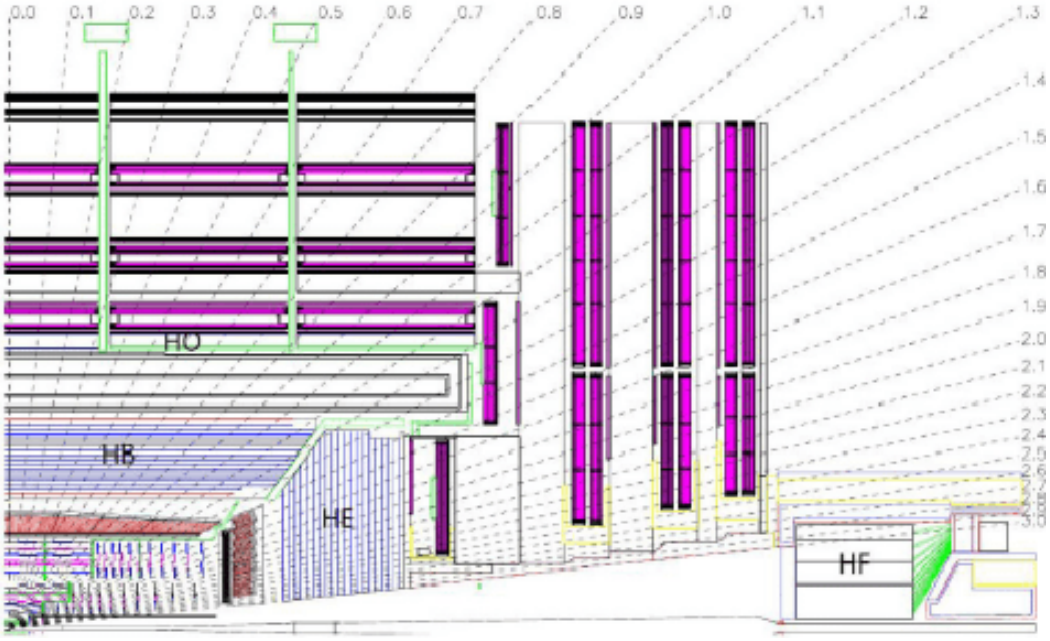

Figure 2.7: Longitudinal view of the CMS detector showing the HCAL subdetectors. [19]

The energy resolution in the dierent regions of HCAL can be parametrized using a stochastic and a constant term, as follows:

$$\left(\frac{\sigma_E}{E}\right)^2 = \left(\frac{90\%\ Gev^{1]2}}{\sqrt{E}}\right)^2 + (4.5\%)^2 \qquad \text{in the barrel/endcap} \qquad (2.6)$$

$$\left(\frac{\sigma_E}{E}\right)^2 = \left(\frac{172\%\ Gev^{1]2}}{\sqrt{E}}\right)^2 + (9\%)^2 \qquad \text{in the HF} \qquad (2.7)$$

2.8 Muon System

The CMS Muon system purpose is to provide good identification and measuring of the transverse momentum p_T for muons. The system is placed outside the magnetic coil, embedded in the return yoke, to fully exploit the 1.8 T return ux as shown in Fig 2.8.The p_T measurement is based on the bending at the magnet point assuming the interaction point as the origin. The muons produced are measured in the tracker and the muon system.For low p_T muons the overall momentum resolution is dominated by the tracker , while for $p_T > 200$ GeV the measurement are obtained by combining the two systems.

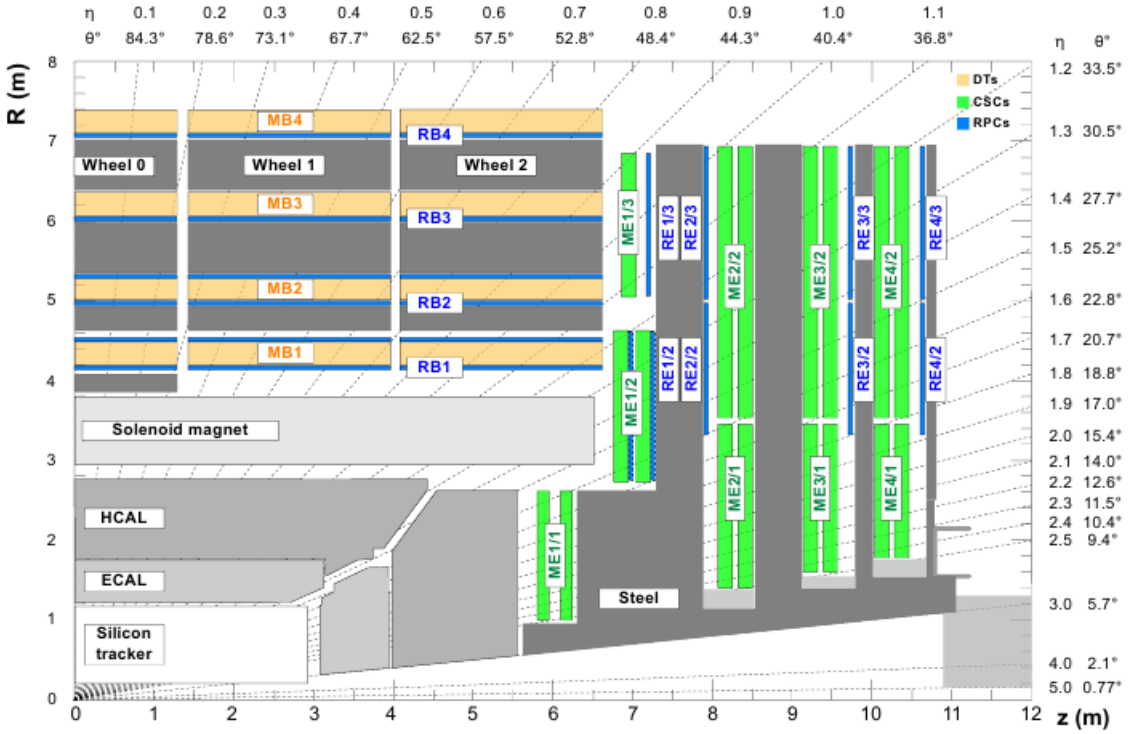

Figure 2.8: Schematic representation of the CMS electromagnetic calorimeter. [21]

The muon interaction with matter is very weak, as they pass through out all sub-detectors after loosing only a small fraction of their energy. The CMS muon system has a three main functions: muon identification ,muon momentum measurement and triggering. It composed of three types of gaseous detectors , which are installed in the barrel and endcaps region of the CMS detector. All of these gaseous detectors with their η coverage is shown in Fig. 2.9 [22].
The muon system covers region $|\eta| < 2.4$. The three detectors are based on different technologies: Drift Tube (DT) chambers in the barrel, Cathode Strip Chambers (CSC) in the endcaps and Resistive Plate Chambers (RPC) to complement the rst two systems. They are described briefly in this section.

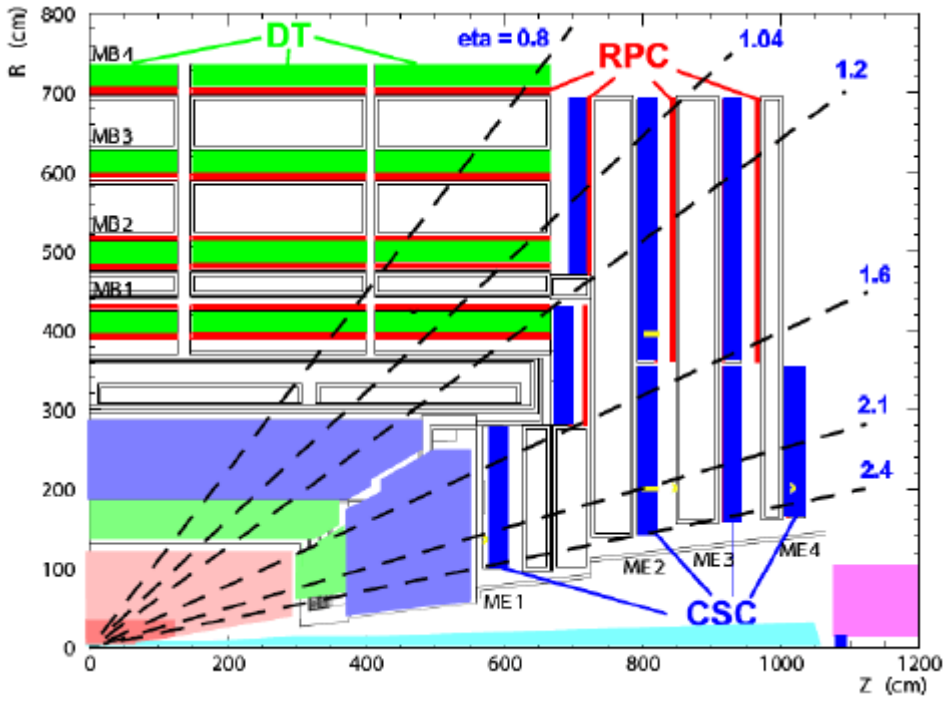

Figure 2.9: Layout of one quadrant of the CMS muon detectors in the r-z plane [21]

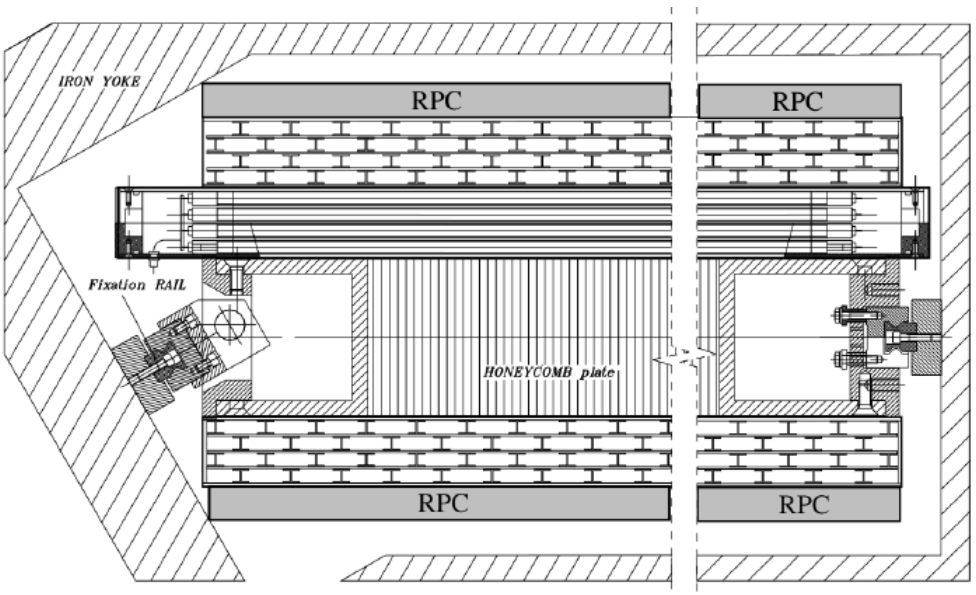

Figure 2.10: Graphic representation of a Drift Tube chamber in the r- plane [23]

2.8.1 Drift Tube chambers

The Drift Tube chambers (DT), Fig.2.10 are a collection of chambers that occupied the barrel region of the muon system, They are allocated in five separate wheels distributed along the z- axis, which covers region $|\eta| < 1.2$. This corresponds to the barrel region where the neutron induced background , residual magnetic field and the total muon rate are low. Each wheel composed of four stations of DT chambers are mounted in the radial direction and intersect with the the magnet return yoke. The three inner stations contains twelve DT chambers per wheel , while the forth station has contains 14 chambers per wheel. The DT chambers are shifted in Φ direction in order to , in order to provide full azimuthal coverage of the barrel muon system. The DT stations are positioned at r = 4.0, 4.9, 5.9, and 7.0 m and consist of 12 sectors, each covering 30 degree in ϕ.The maximum drift length is 2 cm, the point resolution is 200 μm and the precision in ϕ is 100 μm with 1 mrad direction resolution.

2.8.2 Cathode Strip Chambers

The Cathode Strip Chambers (CSCs) are trapezoidal in shape (see Fig 2.11) and have a 6 gas gaps. In each gap there is a plane of radial cathode strips complemented with a plane of anode wires which is perpendicular to the strips. The CSCs strips are extended in radial direction and provide a measurement in Φ direction and anode wires are running in the azimuthal direction providing measurement along the z-axis. The outermost station of the CSCs , the ME4, contains a single ring of 18 chambers. In total, the CSC is comprised of 468 chambers, with 220,000 cathode strips and 180,000 anode readout channels.

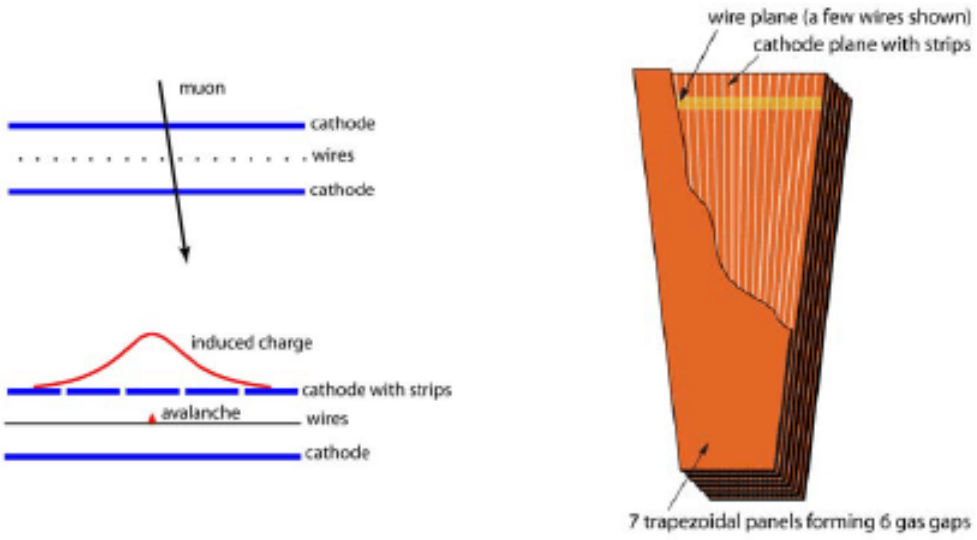

Figure 2.11: The layout of a Cathode Strip Chambers [24]

2.8.3 Resistive plate chambers

The Resistive plate chambers (RPCs) is a gaseous parallel-plate detectors that combine adequate spatial resolution with very precise time measurements. They are mounted on top of the DT chambers and CSCs in the region of $\eta < 1.6$. The RPCs provides information in a much improved timing resolution compared with the DT and CPC chambers[25].
The RPC consists of a double-gap chamber. And in each gap there are two plates operated as electrodes contains the gas mixture. The passage of the charged particle through the chamber allows to measure the time and position of hits by using the read-out strips which are mounted in between the two chamber gaps. This chamber strips are disposed along the beam direction in the barrel RPC region and in the radial direction in the in the RPC endcap region.
The interval between two consecutive LHC bunches is 25 ns which is much higher than the time resolution of the RPC , based on that , the mean function of the the RPC is measuring the bunch-crossing associated to a given muon hit and in providing this information to the trigger system. And together with the trigger , hits are measured in separate chambers to determine the trajectory, and thus the transverse momentum, of a track candidate[20].

2.9 Trigger System

Due to the LHC working conditions, it imposes several constrains on the design of the trigger system, mainly due to the radiation enviroment and large data rate. The LHC collisions occurs at the center of mass energy of 14 TeV, and has a very high interaction rate $\approx 10^9$. The LHC designed luminosity is $10^{34} cm^{-2} sec^{-1}$. Typically around 20 or more simultaneous events are expected. And since it is impossible to store and process this enormous amount of data associated with the large number of events resulting of these collisions, only way is to select the interesting events for processing. Then a rate reduction is achieved for the events with known physics [25].
The detectors are required to have a good time resolution to keep a seprate information for every event. This is can be achieved using a proper trigger system. The trigger main function is to select all the potentially interesting events in presence of huge backgrounds by discarding all the less important processes [26]. It reduces the event rate down to 100 Hz through multiple stage process, and the rate is reduced in two steps, the first step is **Level-1 (L1)** trigger and the second is the **High-Level Trigger (HLT)** [26], as shown in Fig 2.12.

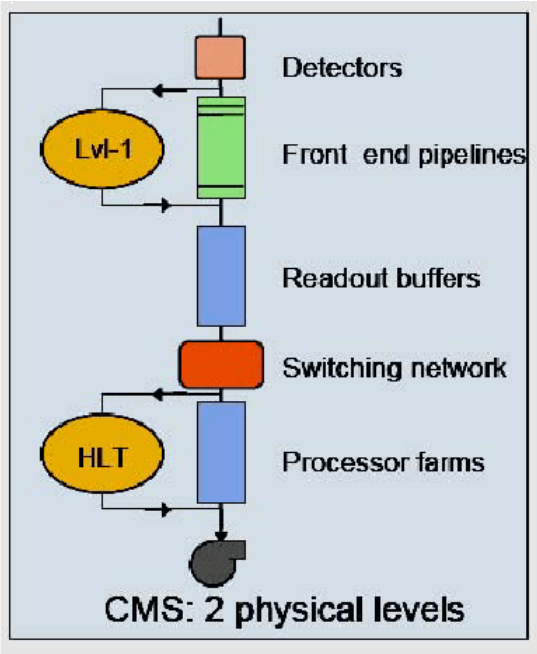

Figure 2.12: Architecture of the CMS Trigger [25]

2.9.1 The CMS Level 1 Trigger

The CMS Level 1 Trigger (L1) function is to take the take the decision to accept or reject an event in a short time of a few microseconds. It is fast self-regulating and selects events with interesting physics, and it picks events with given physics requirement. The trigger objects (electrons , muons and jets) are sorted based in quality information, transverse energy E_T and transversed momentum p_T. The higest rank objects are sent to the global trigger, then applies thresholds and other physics and technical requirements selection criteria. The CMS L1 trigger location information (η, Φ) of the objects.

The top level of L1 trigger is global trigger that receives the information from the calorimeter and muon system. The trigger objects are recorded by the each corresponding sub-detector. The first step of the trigger system is to produce the trigger primitives which is the trigger information collected by the calorimeter and muon system. The Protons bunches colliding with 40 MHz frequency input to level-1 trigger. The L1 then returns a 100 MHz maximum output rate that is the input of the Second Level Trigger.

2.9.2 High Level Trigger (HLT)

The High Level Trigger (HLT) is a software based trigger , and it has a very long processing time compared with the L1. The processing is done using commercial computers clusters . The HLT algorithms access all data from all CMS sub-detectors including the tracker with full resolution. The HLT algorithm calculates quantities with resolution comparable to the final state of the detector. And the output quantities have better resolution. The maximum HLT input rate is 100 MHz and the output rate is about 100 Hz [20].

Chapter 3

Compact Muon Solenoid Silicon Tracker

3.1 Introduction

The inner tracking system is designed for the aim of measuring the trajectories of charged particles precisely as much as possible. CMS was foreseen to use two different detector technologies for the central strip tracking, the silicon based strip detector and micro strip gas chambers. But later in 1999 a full silicon based solution was chosen for the entire tracking device , because the dropping silicon sensors price and the superior radiation hardness. CMS makes use of three layers of silicon pixel detectors and ten layers of silicon strip detectors covering a sensitive silicon area of approximately 200 m^2.In total 1,440 silicon pixel detector modules and 15,148 silicon strip detector modules were built, tested and commissioned on different detector substructures inside the CMS tracker volume.
A detailed overview of the CMS Silicon Tracker (from which much of the material in the following sections is obtained) may be found in [31].

3.2 Layout of the silicon tracker

In three dimensions space , two or three high precision space points are delivered by the tracker pixel system. And starting from the interaction points , particles transverse cross three layers of hybrid pixel detectors at the radii 4.4 cm, 7.3 cm and 10.2 cm. In the endcap region there are two discs which complete the pixel based detector part. And a total of 66 million pixel channels are covering area of 1 m^2. After the particles transverse the pixel layers they enters the silicon strip system. The silicon sttrip system composed of four components as explained before in chapter 2. They are the Tracker Inner Barrel (TIB), Tracker Inner Disks (TID), Tracker Outer Barrel (TOB), two Tracker End Caps (TEC)) composes the strip based system. The inner barrel and inner disks provides Φ measurements in the r < 55 region using 320 μm thick silicon strip sensors.The strips are parallel to the beam axis in the barrel and radially to the beam axis in the end caps. The single point resolution of the strip detectors in the inner part is in the range between 23 μm and 35 μm. There are six outer barrel layers use a 500 μm thick silicon sensors with strip pitches between 122 μm and 183 μm, they

provides six Φ measurements with single point interaction between 35 μm and 53 μm. And the outer barrel covers the radial part up to 116 cm and -118 < z < 118. Two tracker end caps closes the both sides covering the region 124 <|z| < 282 cm and 22.5 < r < 113.5 cm. And each endcap is a nine disks carrying up to seven detector modules. The rings from 1 to 4 carries 320 μm thick silicon sensors, and rings from 5 to 9 carries 500 μm thick silicon sensors. Each endcap can deliver up to nine Φ measurements for every transverse particle depending on the range of η. Fig 3.1 shows a cross section of the silicon tracker.

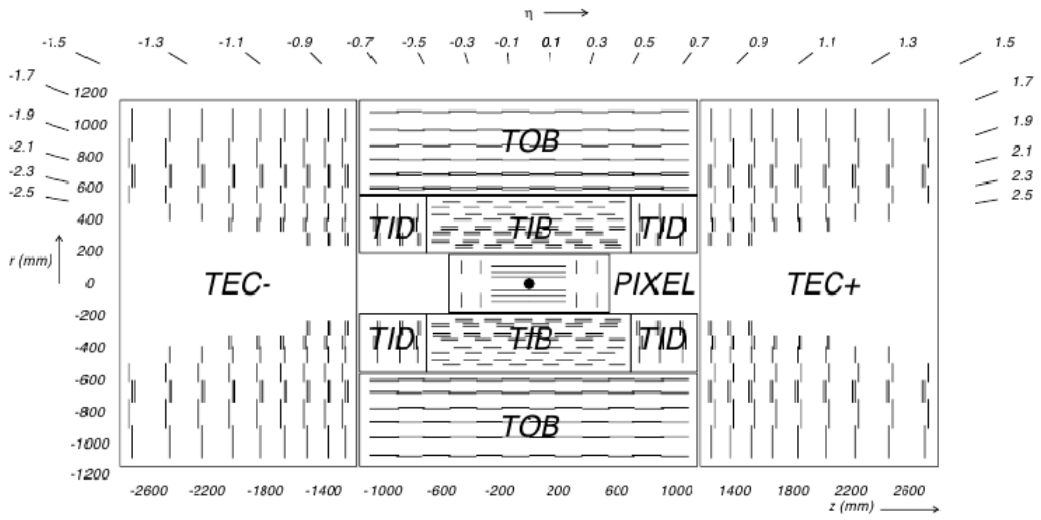

Figure 3.1: Layout of the CMS silicon tracker [17]

For the purpose of providing Perice measurement of a second coordinate, a stereo modules are mounted back-to-back with a stereo angle of 100 mrad to regular modules in some cases. Fig 3.1 shows the position of stereo modules.For the z measurement it is done in the barrel region with the first two layes and rings of TIB M TID and TOB. And in the endcap region the rings 1,3 and 5 are equipped with stereo modules providing an additional measurement of r. The expected number of measured hit positions for traversing particles as a function of is shown in gure 3.2.

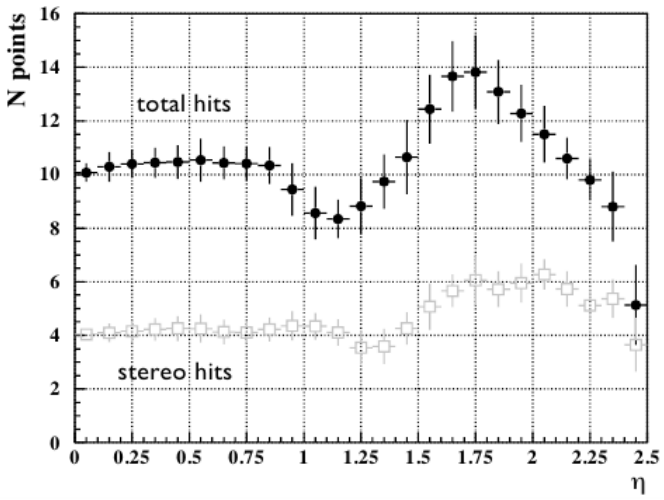

Figure 3.2: The number of measured hit positions as a function of the pseudo-rapidity [30]

3.3 Silicon strip detector modules

A CMS silicon strip detector module is a hybrid object composed of different components. Each module is carrying either one thin 320μm or two thick 500 μm silicon sensor. The modules are supported by carbon or graphite frame. this support is depending on the position of the module in the tracker. And a Kapton layer is used to insulate the silicon sensor from the supporting frame. The Kapton layer is used also to provide electrical connection to the silicon sensor back plane.The module frame carries the front-end hybrid and the pitch adapter necessary to adapt the front-end chip readout pitch to the strip pitch on the silicon sensor [30].Fig 3.3 shows All different modules used in the tracker endcap.

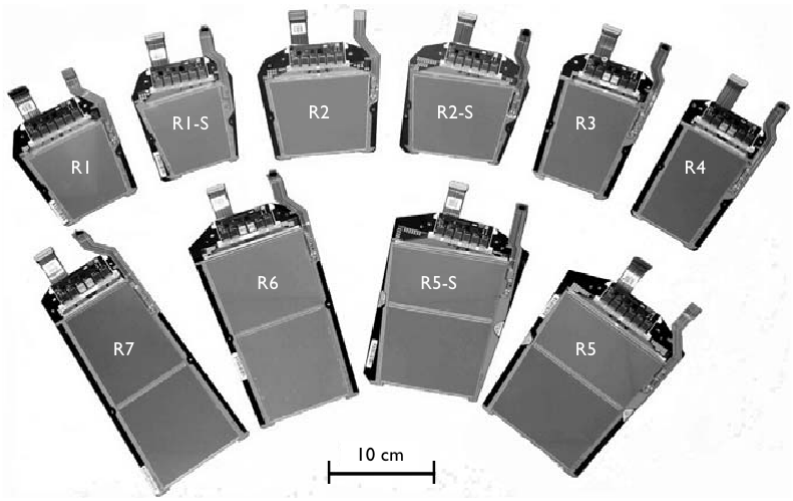

Figure 3.3: tracker endcap modules types [31]

3.4 Radiation hardness

The main feature which prefer the decision for using silicon tracker was the radiation hardness. The silicon strip tracker will suffer from an enormous particle ux during its life time of 10 years and after an integrated luminosity of approximately 500 fb^{-1}.Modules in TID/TIB will experience a ux of up to 1.8×10^{14} 1-MeV-neutron-equivalent per cm^2, and 0.5×10^{14} 1-MeV-neutron-equivalent per cm^2 for the TOB modules there will be less radiation damages in this detector region. The two regions can be distinguished with respect to the main particle types that cause the radiation damages depending on the distance from the beam axis. For the inner barrel region up to 50 cm he dominant fraction will come from fast hadrons, while for the outer tracker region the main part will come from neutrons back scattered off the electromagnetic calorimeter."After irradiation annealing was simulated by heating the detector modules at 60∘C for about 80 minutes. Reverse annealing was avoided by storing the detector modules in a freezer at approximately -20∘C. As expected the full depletion voltage increased with the ux but stayed well below 500 V"[31].

3.5 Tracker substructures

3.5.1 Tracker Inner Barrel

Tracker Inner Barrel (TIB) consists of four concentric rings made of carbon bre at radii of 255.0 mm, 339.0 mm, 418.5 mm and 498.0 mm from the beam axis with a length

of 1,400 mm parallel to the beam. ON the two inner layers there are a stereo modules with a strip pitch of 80 μm are mounted, while the outer layers mounted to single sided modules with strip pitch of 120 μm.Each of the four cylinders is subdivided into four parts , called half shells. Each one of this half shells is self contained system with respect to electrical connections and cooling which has the advantage that one half shell can be fully assembled and tested before integration in the nal system optimizing the tracker resources. Both ends of the TIB sub-detector are connected to which called service cylinder that provides all service connections to a service distribution disk, the so called margherita as shown in Fig 3.4.

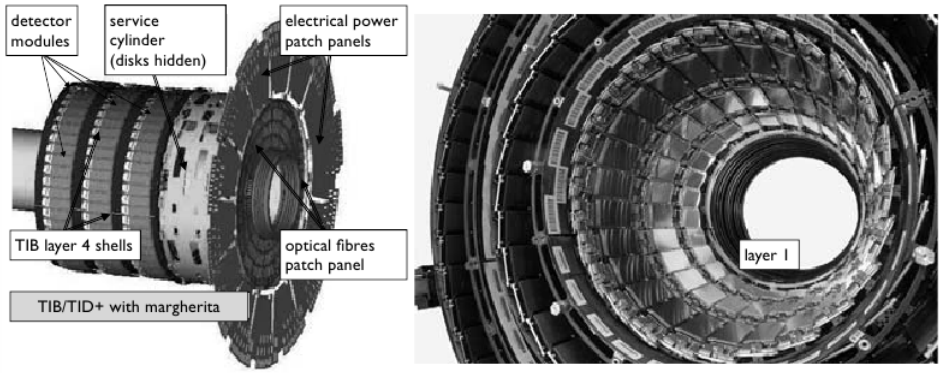

Figure 3.4: Integrated TIB modules on half shells [31]

3.5.2 Tracker Inner disks

The TID consists of three disks covers the range 800 mm < $|z|$ < 900 mm which carrying three rings of modules that forming a sensitive area between the region 200 mm < r < 500 mm. Like the TIB the two inner rings stereo modules are mounted while the outer ring of single sided modules. In both TIB/TID all detector modules are mounted directly on a carbon bre structures as shown in Fig 3.4.

3.5.3 Tracker Outer Barrel

The TOB has a detector modules integrated on 688 rods, similar to the TIB string the rods are inserted in a single mechanical TOB structure called TOB wheel. There are f Three inner and outer car- bon bre composite cylinders support four identical disks also made from carbon bre with a core of aramid-bre honeycomb[31]. There are 344 holes on the disks allows for the rod insertion with each rod supported with two disks. The TOB wheel has a legnth of 218 cm long and cover the region 555 mm < r < 1160

mm. And the wheel rods forms a six layers around the beam axis at distances of 608 mm, 692 mm, 780 mm, 868 mm, 960 mm, and 1,080 mm. The rods are shifted by ± 16 mm from layer to layer to achieve hermetic coverage.

3.5.4 Tracker Endcaps

The Tracker Endcaps are two identical endcap detectors Called TEC+ and TEC- , this naming is according to their position along the beam axis. Both sides of the tracker are closed by a 3200 detector modules. The tracker endcap covers region of 22.5 cm < r < 113.5 cm and 124 cm <|z| <. There are a subdetectors called petals are mounted on nine nine disks per end cap and carry the individual detector modules that are arranged in rings. And like TOB and TIB there are two additional disks to provide tracker termination and the detectors modules are combined with the same idea pf rods and strings.
A U shaped carbon fibre are joined together along the outer radius disks. There are a fibre profile for each endcap which make a role of holding for all services." All disks are made from a carbon bre/honeycomb structure covered on both sides by 0.4 mm thin carbon bre skins and are linked to the inner support tube at four points" [31].

3.6 Laser Alignment System

A Laser Alignment System is required for the process on aliening the individual tracker sub-components with respect to each other and also to provide a connection to the muon system. For this purpose, some of the endcaps modules are infra red laser transparent. The position of the laser beam can be measured using the silicon sensors. On rings 4 and 6 on back petals there are special alignment modules. The laser beam penetrating ring 4 in both TECs connects the end caps with TIB and TOB. Light is reected to modules of the inner TOB layer and the outer TIB layer. For providing the connection to the muon system, another laser beam is used. Fig 3.5 shows a layout of the Laser Alignment Syestem.

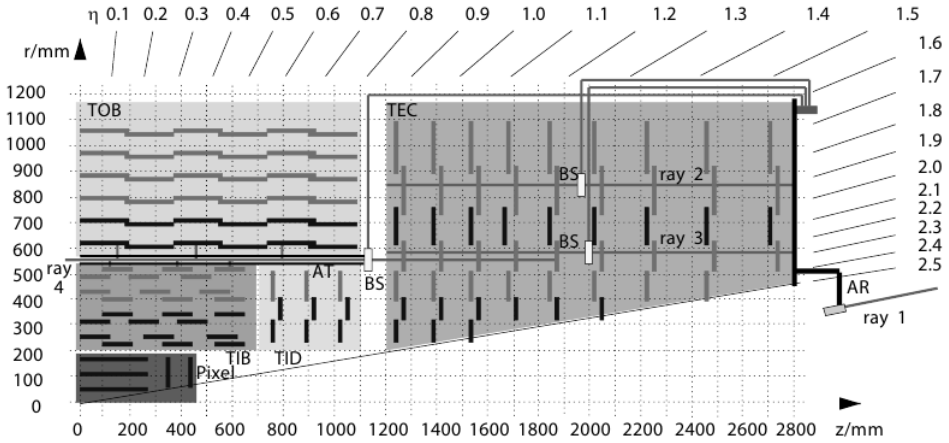

Figure 3.5: r-z projection Layout of the laser alignment system [32]

3.7 Cooling system

The tracker support tubes faces the electromagnetic calorimeter, which require a high stable temperature to operate at excellence performance. The electromagnetic calorimeter outside temperature is 291 ± 277 Kelvin. The tracker volume needs to be cooled to below 263 Kelvin. This thermal gradient in such small distance can be realised by an active thermal screen. Its purpose is to guaranties a temperature below 263 Kelvin inside the silicon tracker volume even when the sub-detectors and their cooling are switched off, and a temperature above 285 Kelvin on the outer surface of the support tube in order to avoid condensation. This thermal screen consists of 32 panels. The cooling progress is a cooling uid circulated inside in a thin aluminum plate whilst, separated by 8 mm of Rohacell foam, with several polyimide-insulated resistive circuits are powered to heat the outer surface to the required temperature. The system is feed-back controlled using 64 temperature sensors.

Chapter 4

Strip Hit Resolution Study

4.1 Tracker Material Study

Analysis is presented to study the material in the Tracker system with nuclear interactions from proton-proton collisions recorded by the CMS experiment at the CERN LHC. The data correspond to an integrated luminosity of 7.3 pb^{-1} at a centre-of-mass energy of 13 TeV collected at 3.8 Tesla magnetic field. With reconstructed nuclear interactions we observe the structure of the material, including beam pipe, in the Tracker system.

4.2 Results

4.2.1 Tracker material study:

Nuclear Interaction is the interaction of hadrons (pions, kaons, protons,...) with the material of the Tracker System. Study of Nuclear Interaction helps to describe Tracker material, which could improve resolution of tracker objects.To reconstruct Nuclear Interaction we request at least 3 coming or out-coming charge tracks in the vertex of nuclear interaction. Tracks are requested to be well reconstructed.

Fig. 4.1 shows Nuclear Interaction for the Run2015B data at 13 TeV, (x,y) plane, zoomed in the beam pipe region, for the barrel part (IzI < 20 cm). Black circle with radius around 2.25 cm corresponds to the beam pipe. It is shifted from the central value of the detector. Grey circle with radius around 3.7 cm corresponds to the Pixel Shield. Structure with radius around 4.2-4.7 cm corresponds to the 1st layer of the Pixel. White circle with radius 1.8 cm corresponds to the reconstruction cut for the nuclear interaction

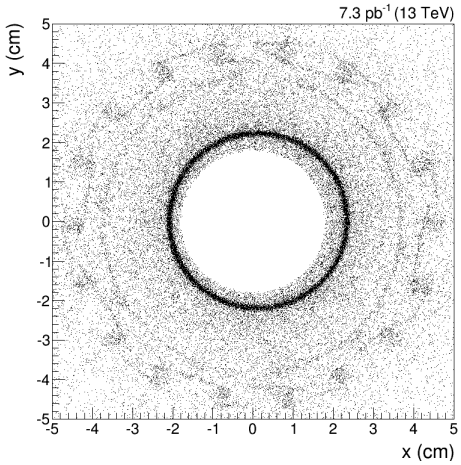

Figure 4.1: Nuclear Interaction for Run2015B data at 13 TeV

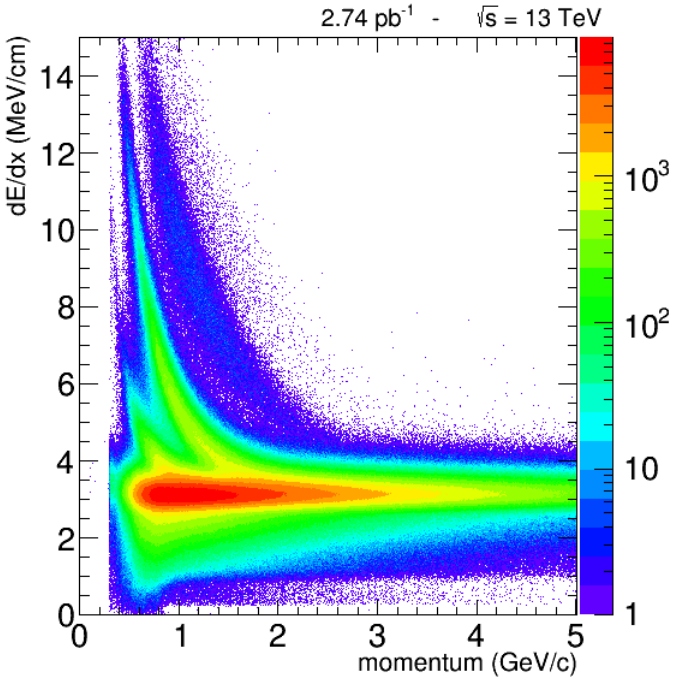

Figure 4.2: Strip performance plots

The commissioning and calibration of the tracker allow to distinguish the particles using the dE/dx information. This quantity relies significantly on the gain calibration. Run 2 results of High Purity Tracks with $|d\theta| < 0.25$ cm and $|dZ| < 0.5$ cm and 12 single-sides strip hits have been used. For each track an average of the square-root of the dE/dx of the strip hits is computed and used as an estimator of the dE/dx of the Fig. 4.3 shows distribution of dE/dx vs momentum using the Pixel-Less Harmonic-2 estimator. From right to left we can clearly see the Deuteron, Proton and Kaon bands

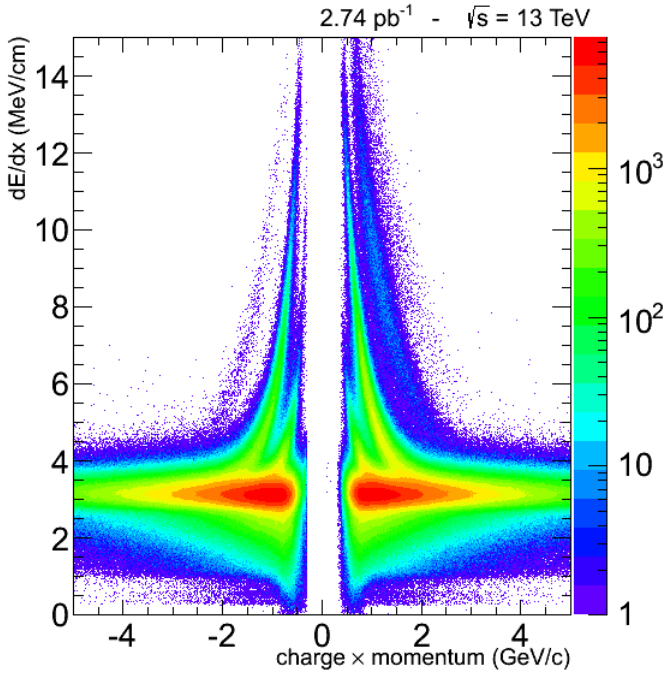

Figure 4.3: distribution of dE/dx vs charge times momentum

4.2.2 Hit Efficiency

Fig. 4.4 shows the hit efficiency is computed from this selection

- Events with less than 100 tracks.
- Use "combinatorialTracks" with at least 8 hits.
- Trajectories that fall within sensor acceptance. Excludes bonding region for modules with 2 sensors.
- Known bad modules are excluded from the measurement.

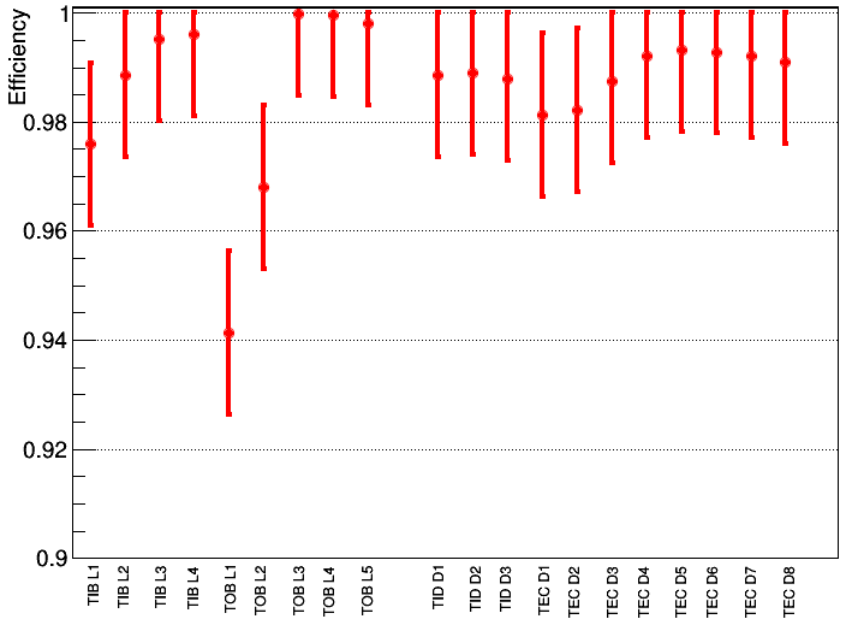

Figure 4.4: Hit Efficiency for the selection

The module is considered as efficient if the distance between the trajectory crossing point and the cluster is less than 15 strips. They also have to fall in strips read by the same APV. For double layers, both are taken into account. The average efficiency is computed. Systematic uncertainties cover possible biases of the method.

4.2.3 Strips Hit Resolution

The full dataset of 2016 is used to measure the strips hit resolution for TOP and TIB for both CMS data and Monte-Carlo(MC).
Fig. 4.5 shows the strip hit resolution in TOB (2) for data in blue and QCD sample in red. The large error bars due to leak of statistics. The discrepancy seen between data and MC is due to the difference in the used tag. That is used to reconstruct data and MC

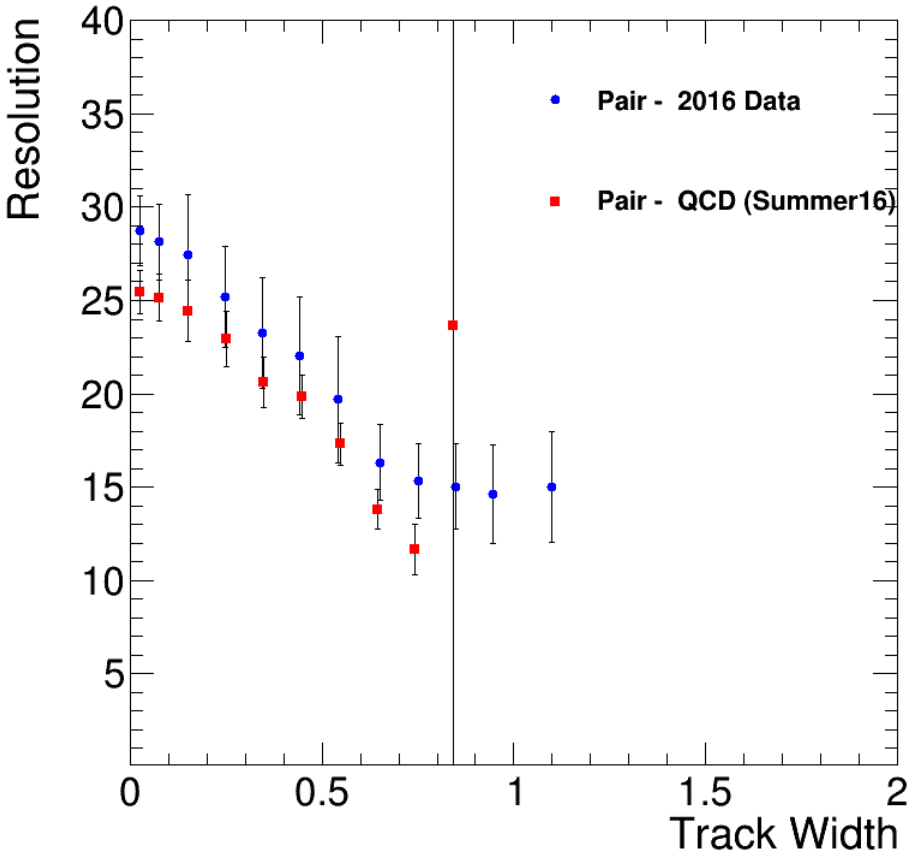

Figure 4.5: strip hit resolution in TOB (2)

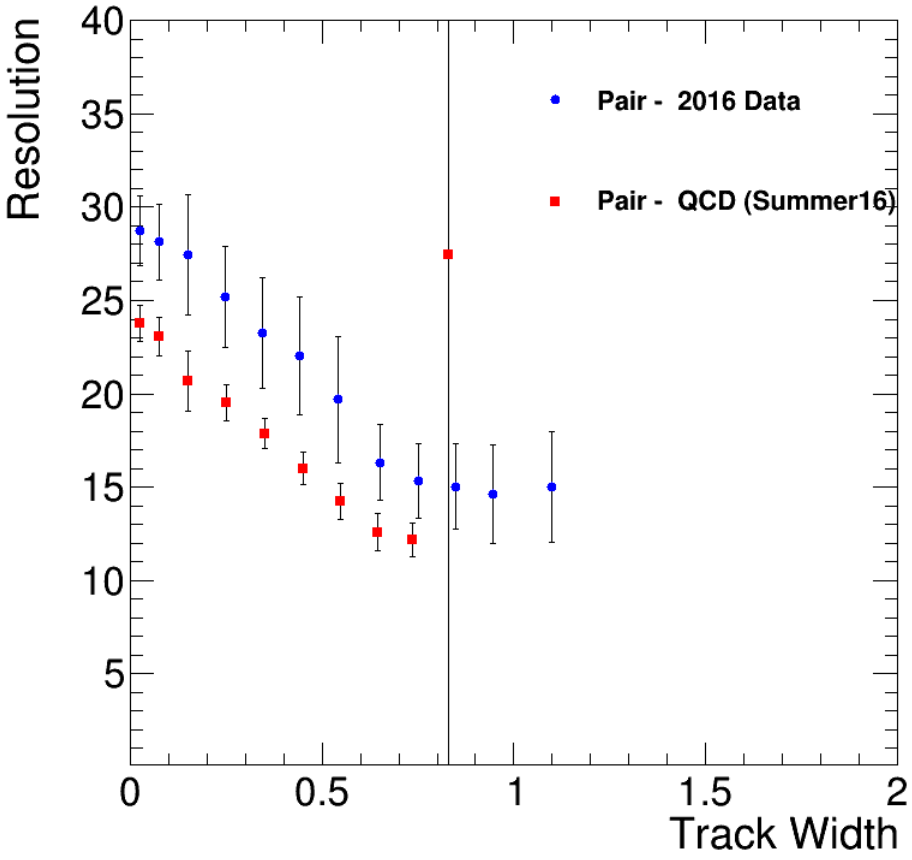

Figure 4.6: strip hit resolution in TOB (1)

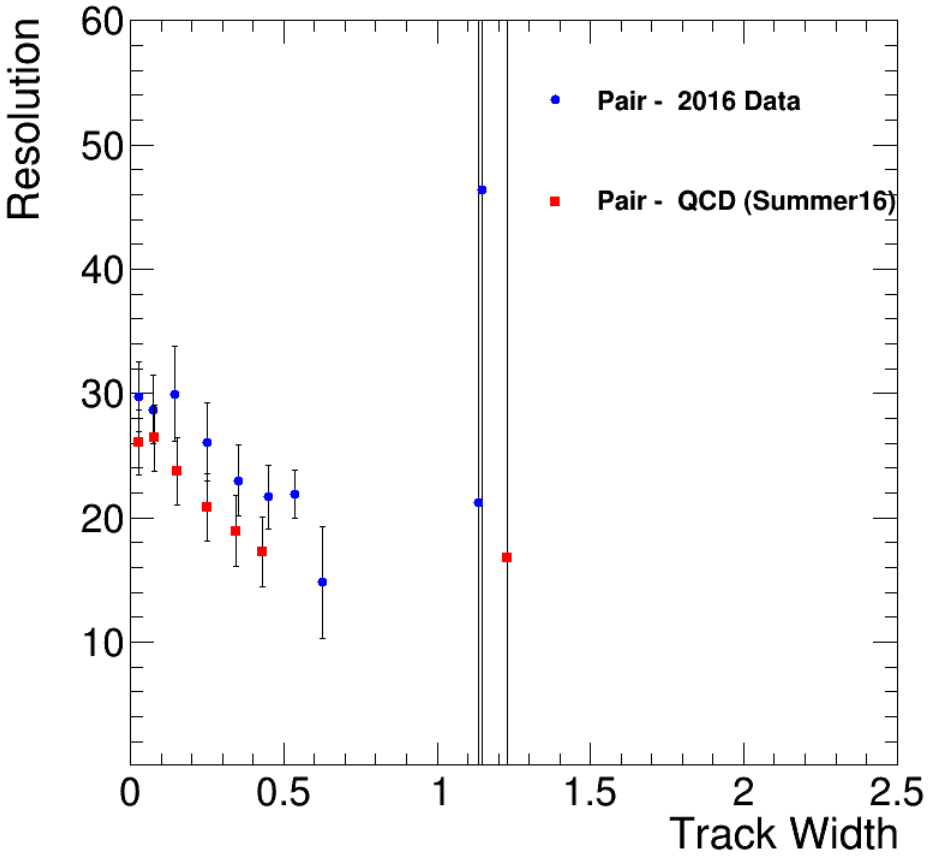

Figure 4.7: strip hit resolution in TIB (2)

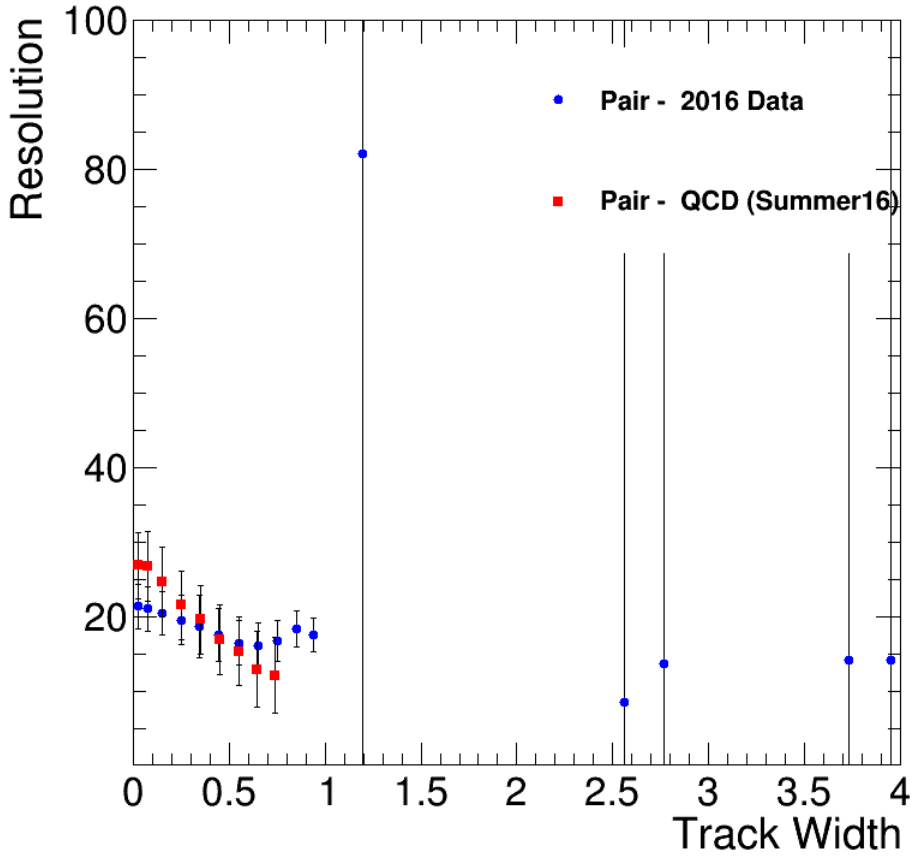

Figure 4.8: strip hit resolution in TIB (1)

In all the previous plots , which represent the result of the study for the strip hit resolutions for different layers. More statistics is needed for more accurate measurements. The observed discrepancy between the data and Monto-Carlo simulation is due to the difference in the detector geometry version used in data and the Monto-Carlo samples. The plots here are for four different layers for CMS silicon tracker , as shown before in Fig 3.1.

References

[1] "CERN|Accelerating science." http://www.cern.ch

[2] R. Assmann et al., “A brief history of the LEP collider”, Nucl. Phys. Proc. Suppl. **109B** (2002) 17–31.

[3] "Atlas Experiment." http://atlas.cern

[4] "CMS Experiment." http://cms.cern/

[5] "Alice Experiment." http://alice-collaboration.web.cern.ch/

[6] "LHcb Experiment." http://lhcb-public.web.cern.ch/lhcb-public/

[7] Alison, J., Kroll, J. (n.d.). The Road to Discovery : Detector Alignment, Electron Identification, Particle Misidentification, WW Physics, and the Discovery of the Higgs Boson. Pennsylvania U: UMI Dissertation Publishing.

[8] Tahir, N. A., J. Blanco Sancho, A. Shutov, R. Schmidt, and A. R. Piriz. "Impact of High Energy High Intensity Proton Beams on Targets: Case Studies for Super Proton Synchrotron and Large Hadron Collider." Physical Review Special Topics - Accelerators and Beams 15.5 (2012): n. pag. Web.

[9] Lyndon R. Evans and Philip Bryant. “LHC Machine”. In: J. Instrum. 3 (2008). This report is an abridged version of the LHC Design Report (CERN-2004-003), S08001. 164 p.

[10] Shoaib, M. (2016). Single top-quark production cross-section measurement in association with Z boson and performance studies of the RPCs with the CMS detector using 8 TeV pp Single top-quark production cross-section measurement in association with Z boson and performance studies of the RPCs with the CMS detector using 8 TeV pp collisions at the LHC collisions at the LHC (Master’s thesis, Quaid-I-Azam University , Islamabad).

[11] C. Eck et al., LHC computing Grid: Technical Design Report. Version 1.06 (20 Jun 2005). Technical Design Report LCG. CERN, Geneva, 2005.

[12] Herr, Werner, and B Muratori. "Concept Of Luminosity". CERN Document Server. N.p.

[13] **CMS** Collaboration, "The CMS experiment at the CERN LHC", JINST 3 (2008) S08004, doi:10.1088/1748-0221/3/08/S08004.

[14] Naturalness confronts nature: searches for supersymmetry with the CMS detector in pp collisions at $\sqrt{s}$ = 8 and 1313 TeV - Duarte, Javier Mauricio FERMILAB-THESIS-2017-02

[15] S. Chatrchyan et al. "The CMS experiment at the CERN LHC". In: JINST 3 (2008), S08004. DOI: 10.1088/1748-0221/3/08/S08004.

[16] Single top-quark production cross-section measurement in association with Z boson and performance studies of the RPCs with the CMS detector using 8 TeV pp collisions at the LHC -Shoaib, Muhammad , Hoorani, Hafeez R CERN-THESIS-2016-275

[17] D . Sprenger, M . Weber, R. Adolphi, R. Brauer, L. Feld, K. Klein, A. Ostaptchuk, S . Schael , and B. Wittmer , Validation of Kalman Filter alignment algorithm with cosmic-ray data using a CMS silicon strip tracker endcap, JINST 5 (2010) P06007,

[18] **CMS** Collaboration, S. Chatrchyan et al. , Description and performance of track and primary-vertex reconstruction with the CMS tracker, JINST 9 (2014) , no. 10

[19] B . Isildak, Measurement of the dierential dijet production cross section in proton-proton collisions at $\sqrt{s}$ = 7 TeV

[20] Measurement of the Higgs boson properties and search for new resonances using W^+W decays with the CMS detector - Viliani, Lorenzo , Ciulli, Vitaliano R **CERN**-THESIS-2017-019

[21] Searches for top-antitop quark resonances in semileptonic final states with the CMS detector - Missiroli, Marino CERN-THESIS-2017-014, **CMS**-TS-2017-005

[22] **CMS** Collaboration, "The CMS muon project", Technical Design Report, CERN-LHCC-97-032 (1997).

[23] **CMS** Collaboration, "The CMS experiment at the CERN LHC", JINST 3 (2008) S08004.

[24] The **CMS** Collaboration, The CMS experiment at the CERN LHC, JINST 3, S08004 (2008) .

[25] **CMS** Collaboration, "The performance of the CMS muon detector in proton-proton collisions at $\sqrt{s}$ = $7 TeV at the LHC$], $JINST 8(2013)P11002$

[26] The **CMS** Collaboration, Concept of the First Level Global Trigger for the CMS Experiment at LHC Nucl. Instr. Meth. A473/3, 2001

[27] The **CMS** Collaboration, The TriDAS project, technical design report. Volume 2: Data acquisition and high-level trigger technical design report, CERN-LHCC-2002-026

[28] **LHC** Beam Stability and Feedback Control - Orbit and Energy - - Steinhagen, R.J. CERN-THESIS-2007-058

[29] Precise measurement of the charged B meson mass at the LHCb experiment - Emiliano , Furfaro , Giovanni, Carboni **CERN**-THESIS-2017-028

[30] **CMS** Collaboration , R. Adolphi et al. , The CMS experiment at the CERN LHC, JINST 3 (2008) S08004

[31] Pooth, Oliver. The CMS Silicon Strip Tracker Concept, Production, and Commissioning. Wiesbaden: Vieweg Teubner Verlag / GWV Fachverlage GmbH, Wiesbaden, 2010. Print.

[32] R. Adolphi, Construction and calibration of the laser alignment system for the CMS tracker, PhD thesis, RWTH Aachen, 2006